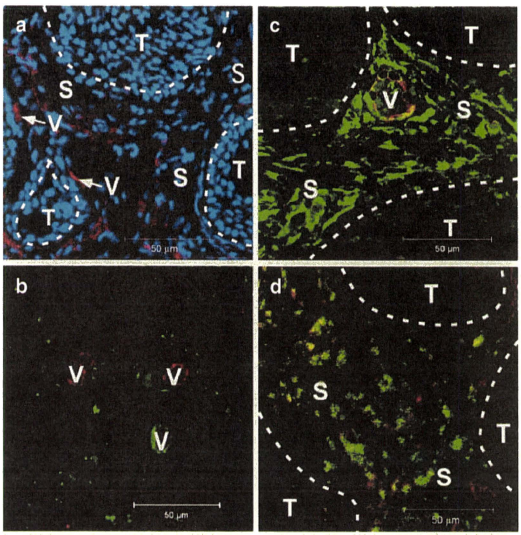


**Fig. 8.** EGFP transfection into subcutaneous tumors of pancreatic adenocarcinoma cells, BxPC3, *via* systemic route. Each micelle sample was prepared at a Lys/Phosphate=2, and intravenously injected through the tail veins of the mice (20 μg pDNA/mouse). **a** Histology of BxPC3 xenograft as a model of poorly differentiated pancreatic tumor tissue. *Blue*: nucleus stained with Hoechst 33342, *red*: PECAM-1 as an endothelial marker stained with Alexa647-conjugated secondary antibody against anti-PECAM-1 antibody (regions *T*, *S*, and *V* indicate nests of tumor cells in tumor tissues, thick fibrotic tissue in the stroma, and blood vasculature, respectively). **b** EGFP expression by PAsp36(DET)Lys50 polyplex micelle without TβR-I inhibitor; **c** EGFP expression by PAsp36(DET)Lys50 polyplex micelle with TβR-I inhibitor; **d** EGFP expression by PLys71 polyplex micelles with TβR-I inhibitor.

micelles in combination with TβR-I inhibitor did not show detectable EGFP expression in the liver and lung under the tested conditions (data not shown). Fig. 8d shows the result obtained for the PLys71 polyplex micelles with TβR-I inhibitor. Obviously, the EGFP expression by the PAsp36 (DET)Lys50 polyplex micelles was much more remarkable than that with the PLys71 polyplex micelles, suggesting that the integration of the PAsp(DET) segment into the polyplex micelles is effective even in the transfection by systemic administration. Detailed observation of the fluorescence images revealed that the EGFP expression by the polyplex micelles was located mainly around PECAM-1-positive vascular endothelial cells. As typically shown in Fig. 8a, the tumor stroma grows around the nests of tumor cells in BxPC3 subcutaneous xenografts, and blood vasculature exists inside the stroma. Therefore, a major part of the EGFP expression in the BxPC3 tumor by PAsp36(DET)Lys50 polyplex micelles was not from BxPC3 cells *per se*, but from cells in the stroma including vascular endothelial cells and fibroblasts.

## DISCUSSION

In the present study, polyplex micelles with an endosomal escape layer were prepared from a triblock copolymer for the purpose of transfection into solid tumors through systemic routes. The triblock copolymer was composed of three tandemly aligned functional segments as follows: PEG for biocompatibility, PAsp(DET) for efficient endosomal escape, and PLys for pDNA condensation. A series of triblock copolymers, PEG–PAsp(DET)–PLys, with the DP of PLys of approximately 50, was synthesized and used for the preparation of the polyplex micelles, according to the previous results that a DP of approximately 48 was needed for effective transfection with polyplex micelles from PEG–PLys as shown in Fig. 5c as well as for the prolonged circulation of intact pDNA in the blood stream (10). The triblock copolymer, PAsp36(DET)Lys50, as well as the diblock PEG–PLys, PLys48, effectively condensed pDNA to form a polyplex micelle (Fig. 3). The obtained polyplex micelles

from the triblock copolymer were around 80 nm at an $N^+/P$ ratio of 1 or greater (Fig. 4a), thereby having the potential ability to accumulate in tumors through the enhanced permeability and retention (EPR) effect (27). Also, the zeta potential measurement indicated that the excess positive charge of the polyplex micelle from the triblock copolymer was reasonably shielded by a PEG palisade surrounding the polyplex core (Fig. 4b). It should be noted that PEGylation of polyplexes facilitates their penetration into tumor spheroids (15, 16). Hence, the PEG palisade of polyplex micelles from the triblock copolymer may contribute to promoting their permeation into the tumor tissue *via* extravasation as well as to extending their plasma half-life through a steric stabilization effect, leading to appreciable gene expression in the subcutaneous pancreatic tumor tissue as seen in Fig. 8. Note that the xenografted pancreatic tumor, BxPC3, was chosen as our target in this study. Since pancreatic tumors are representative of intractable tumors, which are difficult to treat by conventional therapy, they are an appropriate target for the development of new strategies including gene therapy. However, it is also difficult to deliver exogenous genes to such tumor tissue by gene carriers through an EPR effect, presumably due to their thick fibrotic and hypovascular characteristics. In this regard, the combined use of TβR-I inhibitor, which has been found to decrease pericyte coverage of the endothelium specifically in tumor neovasculature (21), is available for the enhancement of accumulation of nanocarriers of 60–100 nm diameter into the solid tumor. Indeed, the EGFP expression by the polyplex micelles from PAsp36(DET)Lys50 was substantially improved by the intraperitoneal injection of TβR-I inhibitor (Fig. 8b,c). The size of the polyplex micelle was approximately 80 nm, thereby making it suitable for combination with TβR-I inhibitor. As far as we know, this is the first example of effective gene expression in BxPC3 tumors with thick fibrotic and hypovascular characteristics *via* systemic administration of non-viral vectors. In addition, detailed observation of the fluorescence images from sectioned xenografted tumors revealed that the EGFP expression by the PAsp36(DET)Lys50 polyplex micelle combined with TβR-I inhibitor was located mainly around the blood vasculature (Fig. 8c), suggesting that the transfection with the polyplex micelle was not effective for the tumor cells *per se*, but for the cells in the tumor stroma, including vascular endothelial cells and fibroblasts. These results suggest that the penetration of polyplex micelles into tumor microenvironments may still be a major challenge, even with the aid of TβR-I inhibitor for successful systemic transfection directly to the BxPC3 tumor cells. In this regard, for the gene therapy of pancreatic adenocarcinoma with thick fibrotic tissues, the approach of treating the tissues surrounding the nests of tumor cells would be more realistic than that directly targeting tumor cells *per se*, e.g., with a tumor suppressor gene to induce apoptosis. Antiangiogenic gene therapy is one of the typical "indirect" approaches to treating fibrotic tumors, and research in this direction on combination treatment using polyplex micelles and TβR-I inhibitor is now ongoing in our laboratory.

The contribution of the PAsp(DET) segment in the triblock copolymer to improved transfection without increased cytotoxicity was obvious from the results of both *in vitro* and *in vivo* transfection studies (Figs. 5, 8, and Table II). It should be noted that there is no significant difference in cellular uptake between the polyplex micelles from the triblock and diblock copolymers (Fig. 6), even though the former revealed almost one order of magnitude higher transfection efficacy than the latter. This result suggests that the major cause for the facilitated transfection with the polyplex micelles from the triblock copolymer may be in the intracellular stage. Indeed, the CLSM observation clearly revealed the facilitated endosomal escape of pDNA associated with the polyplex micelles from the triblock copolymer (Fig. 7), indicating the availability of PAsp(DET) as an endosomal escape element. PAsp(DET) is likely to form the middle layer between the PEG shell and the PLys/pDNA polyplex core in the micelles, because PLys with higher affinity to pDNA than PAsp(DET) is assumed to undergo preferential condensation of pDNA, relegating the PAsp(DET) segment to the boundary with the PEG layer. Increased freedom of PLys as an outer block with a free chain-end may also contribute to the preferential complexation with pDNA. Note that a similar three-layered structure was previously proposed by us for polyplex micelles prepared from PEG–PAsp(APM)–PLys based on the results of $^1$H-NMR spectroscopy (20). The appreciably higher zeta potential of PAsp36(DET)Lys50 micelles in the region at an $N^+/P$ ratio of 1 or greater is consistent with the formation of a cationic middle layer (Fig. 4b,c) that is not completely shielded by the outer PEG layer. Thus, the PAsp(DET) placed in the middle layer of polyplex micelles should exert endosomal escape ability for efficient transfection through strong buffering and/or a membrane-destabilizing effect based on the unique two-step protonation behavior of the 1,2-diaminoethane unit (13,15). On the other hand, as seen in Fig. 5b, the one order of magnitude lower transfection efficacy obtained by reversing the order of PLys and PAsp(DET) segments in the triblock copolymer is interesting. It is reasonable to consider that arrangement of the PLys segment, with its strong condensing power against pDNA, as the intermediate segment of the triblock copolymer may allow the PAsp(DET) segment to become embedded in the core of the polyplex micelles, resulting in the loss of buffering and/or membrane-destabilizing capacity. The zeta potential of the PEG–PLys–PAsp(DET) systems similar to that of the PEG–PLys systems also supports the disappearance of the intermediate buffering layer in the polyplex micelles from PEG–PLys–PAsp(DET) with the reversed order of the cationic segments (Fig. 4d).

## CONCLUSION

For the achievement of systemic gene delivery to solid tumors with appreciable transfection efficacy, gene carriers are required to exert integrated functions including a stealth property in the blood stream to deliver intact pDNA into tumor tissues and permeate target cells with smooth translocation from endosomal compartments into the cytoplasm, subsequently releasing the pDNA to induce effective transcription. In the present study, to develop a gene carrier with such integrated functions, three segments with distinctive functions; i.e., PEG for biocompatibility, PAsp(DET) for endosomal escape, and PLys for pDNA condensation, were tandemly aligned in a polymer strand to form three-layered

polyplex micelles. The obtained micelles showed one order of magnitude higher transfection efficacy against Huh-7, compared to the micelles from the PEG–PLys diblock copolymer without any segments exerting an endosomal escape function. Notably, the polyplex micelle from the triblock copolymer achieved clear *in vivo* transfection of the EGFP gene in fibrotic pancreatic adenocarcinoma, BxPC3, through systemic administration. It should be emphasized that the EGFP expression in the pancreatic tumor was drastically enhanced by the intraperitoneal injection of TβR-I inhibitor prior to the micelle injection, and thus, the potential for combined therapy using polyplex micelles and TβR-I inhibitor for systemic transfection to solid tumors was clearly evidenced. Furthermore, detailed observation of the immunostained tumor tissues revealed that the EGFP expression by the triblock copolymer micelles was located mainly in the stromal tissues surrounding the nests of tumor cells. These results suggest that the triblock micelle is quite promising for fibrotic tumor treatments by the approach of transfecting the tissues surrounding tumor cells, including fibroblasts and endothelial cells, to express proteins inhibiting tumor angiogenesis.

## ACKNOWLEDGEMENTS

This work was financially supported by the Core Research Program for Evolutional Science and Technology (CREST) from the Japan Science and Technology Corporation (JST) as well as by Special Coordination Funds for Promoting Science and Technology from the Ministry of Education, Culture, Sports, Science and Technology of Japan (MEXT).

## REFERENCES

1. Wiley (2007) Gene Therapy Clinical Trials Worldwide, provided by the *J. Gene Med.* http://www.wiley.co.uk/genetherapy/clinical/ (accessed 17/01/08)
2. D. W. Pack, A. S. Hoffman, S. Pun, and P. S. Stayton. Design and development of polymers for gene delivery. *Nat. Rev. Drug Discov.* **4**:581–593 (2005) doi:10.1038/nrd1775.
3. E. Mastrobattista, M. A. E. M. van der Aa, W. E. Hennink, and D. J. A. Crommelin. Artificial viruses: a nanotechnological approach to gene delivery. *Nat. Rev. Drug Discov.* **5**:115–121 (2006) doi:10.1038/nrd1960.
4. E. Wagner. Strategies to improve DNA polyplexes for *in vivo* gene transfer: Will "artificial viruses" be the answer? *Pharm. Res.* **21**:8–14 (2004) doi:10.1023/B:PHAM.0000012146.04068.56.
5. Y. Kakizawa, and K. Kataoka. Block copolymer micelles for delivery of gene and related compounds. *Adv. Drug Deliv. Rev.* **54**:203–222 (2002) doi:10.1016/S0169-409X(02)00017-0.
6. S. Katayose, and K. Kataoka. Water-soluble polyion complex associates of DNA and poly(ethylene glycol)-poly(L-lysine) block copolymer. *Bioconjugate Chem.* **8**:702–707 (1997) doi:10.1021/bc9701306.
7. M. A. Wolfert, E. H. Schacht, V. Toncheva, K. Ulbrich, O. Nazarova, and L. W. Seymour. Characterization of vectors for gene therapy formed by self-assembly of DNA with synthetic block co-polymers. *Hum. Gene. Ther.* **10**:2123–2133 (1996) doi:10.1089/hum.1996.7.17-2123.
8. Y. H. Choi, F. Liu, J. Kim, Y. K. Choi, J. S. Park, and S. W. Kim. Polyethylene glycol-grafted poly-L-lysine as polymeric gene carrier. *J. Control. Release.* **54**:39–48 (1998) doi:10.1016/S0168-3659(97)00174-0.
9. K. Itaka, A. Harada, K. Nakamura, H. Kawaguchi, and K. Kataoka. Evaluation by fluorescence resonance energy transfer of the stability of nonviral gene delivery vectors under physiological conditions. *Biomacromolecules.* **3**:841–845 (2002) doi:10.1021/bm025527d.
10. M. Harada-Shiba, K. Yamauchi, A. Harada, I. Takamisawa, K. Shimokado, and K. Kataoka. Polyion complex micelles as a vector in gene therapy—pharmacokinetics and *in vivo* gene transfer. *Gene. Ther.* **9**:407–414 (2002) doi:10.1038/sj.gt.3301665.
11. O. Boussif, F. Lezoualc'h, M. A. Zanta, M. D. Mergny, D. Scherman, B. Demeneix, and J. Behr. A versatile vector for gene and oligonucleotide transfer into cells in culture and *in-vivo* polyethylenimine. *Proc. Natl. Acad. Sci. U. S. A.* **92**:7297–7301 (1995) doi:10.1073/pnas.92.16.7297.
12. M. Neu, D. Fischer, and T. Kissel. Recent advances in rational gene transfer vector design based on poly(ethylenimine) and its derivatives. *J. Gene Med.* **7**:992–1009 (2005) doi:10.1002/jgm.773.
13. N. Kanayama, S. Fukushima, N. Nishiyama, K. Itaka, W.-D. Jang, K. Miyata, Y. Yamasaki, U. Chung, and K. Kataoka. A PEG-based biocompatible block catiomer with high buffering capacity for the construction of polyplex micelles showing efficient gene transfer toward primary cells. *Chem. Med. Chem.* **1**:439–444 (2006) doi:10.1002/cmdc.200600008.
14. K. Masago, K. Itaka, N. Nishiyama, U. Chung, and K. Kataoka. Gene delivery with biocompatible cationic polymer: pharmacogenomic analysis on cell bioactivity. *Biomaterials.* **28**:5169–5175 (2007) doi:10.1016/j.biomaterials.2007.07.019.
15. M. Han, Y. Bae, N. Nishiyama, K. Miyata, M. Oba, and K. Kataoka. Transfection study using multicellular tumor spheroids for screening non-viral polymeric gene vectors with low cytotoxicity and high transfection efficiencies. *J. Control Release.* **121**:38–48 (2007a) doi:10.1016/j.jconrel.2007.05.012.
16. M. Han, Y. Bae, N. Nishiyama, and K. Kataoka. Gene delivery with poly(amino acid)-based block catiomer polyplex micelles against multicellular tumor spheroid. *Abstracts of 13th International Symposium on Recent Advances in Drug Delivery Systems*, Salt Lake City, UT, (2007b), pp. 128.
17. D. Akagi, M. Oba, H. Koyama, N. Nishiyama, S. Fukushima, T. Miyata, H. Nagawa, and K. Kataoka. Biocompatible micellar nanovectors achieve efficient gene transfer to vascular lesions without cytotoxicity and thrombus formation. *Gene. Ther.* **14**:1029–1038 (2007) doi:10.1038/sj.gt.3302945.
18. K. Itaka, S. Ohba, K. Miyata, H. Kawaguchi, K. Nakamura, T. Takato, U. Chung, and K. Kataoka. Bone regeneration by regulated *in vivo* gene transfer using biocompatible polyplex nanomicelles. *Mol. Ther.* **15**:1655–1662 (2007) doi:10.1038/sj.mt.6300218.
19. K. Miyata, S. Fukushima, N. Nishiyama, Y. Yamasaki, and K. Kataoka. PEG-based block catiomers possessing DNA anchoring and endosomal escaping functions to form polyplex micelles with improved stability and high transfection efficacy. *J. Control Release.* **122**:252–260 (2007) doi:10.1016/j.jconrel.2007.06.020.
20. S. Fukushima, K. Miyata, N. Nishiyama, N. Kanayama, Y. Yamasaki, and K. Kataoka. PEGylated polyplex micelles from triblock catiomers with spatially ordered layering of condensed pDNA and buffering units for enhanced intracellular gene delivery. *J. Am. Chem. Soc.* **127**:2810–2811 (2005) doi:10.1021/ja0440506.
21. M. R. Kano, Y. Bae, C. Iwata, Y. Morishita, M. Yashiro, M. Oka, T. Fujii, A. Komuro, K. Kiyono, M. Kamiishi, K. Hirakawa, Y. Ouchi, N. Nishiyama, K. Kataoka, and K. Miyazono. Improvement of cancer-targeting therapy, using nanocarriers for intractable solid tumors by inhibition of TGF-beta signaling. *Proc. Natl. Acad. Sci. U. S. A.* **104**:3460–3465 (2007) doi:10.1073/pnas.0611660104.
22. W. H. Daly, and D. Poche. The preparation of *N*-carboxyanhydrides of alpha-amino-acids using bis(trichloromethyl)carbonate. *Tetrahedron Lett.* **29**:5859–5862 (1988) doi:10.1016/S0040-4039(00)82209-1.
23. A. Koide, A. Kishimura, K. Osada, W. -D. Jang, Y. Yamasaki, and K. Kataoka. Semipermeable polymer vesicle (PICsome) self-assembled in aqueous medium from a pair of oppositely charged block copolymers: physiologically stable micro-/nanocontainers of water-soluble macromolecules. *J. Am. Chem. Soc.* **128**:5988–5989 (2006) doi:10.1021/ja057993r.
24. A. Harada, S. Cammas, and K. Kataoka. Stabilized α-helix structure of poly(L-lysine)-block-poly(ethylene glycol) in aque-

ous medium through supramolecular assembly. *Macromolecules*. **29**:6183–6188 (1996) doi:10.1021/ma960487p.

25. A. Harada, and K. Kataoka. Formation of polyion complex micelles in an aqueous milieu from a pair of oppositely-charged block copolymers with poly(ethylene glycol) segments. *Macromolecules*. **28**:5294–5299 (1995) doi:10.1021/ma00119a019.
26. K. Itaka, K. Yamauchi, A. Harada, K. Nakamura, H. Kawaguchi, and K. Kataoka. Polyion complex micelles from plasmid DNA and poly(ethylene glycol)-poly(L-lysine) block copolymer as serum-tolerable polyplex system: physicochemical properties of micelles relevant to gene transfection efficiency. *Biomaterials*. **24**:4495–4506 (2003) doi:10.1016/S0142-9612(03)00347-8.
27. Y. Matsumura, and H. Maeda. A new concept for macromolecular therapeutics in cancer chemotherapy: mechanism of tumoritropic accumulation of proteins and the antitumor agent SMANCS. *Cancer Res.* **46**:6387–6392 (1986).

J|A|C|S
ARTICLES

Published on Web 04/09/2008

# PEG-Detachable Polyplex Micelles Based on Disulfide-Linked Block Catiomers as Bioresponsive Nonviral Gene Vectors

Seiji Takae,[†] Kanjiro Miyata,[‡,⊥] Makoto Oba,[§] Takehiko Ishii,[‡,⊥] Nobuhiro Nishiyama,[∥,⊥] Keiji Itaka,[∥] Yuichi Yamasaki,[†,⊥] Hiroyuki Koyama,[§] and Kazunori Kataoka*[,†,‡,∥,⊥]

*Department of Materials Engineering, Graduate School of Engineering, The University of Tokyo, 7-3-1 Hongo, Bunkyo-ku, Tokyo 113-8656, Japan, Department of Bioengineering, Graduate School of Engineering, The University of Tokyo, 7-3-1 Hongo, Bunkyo-ku, Tokyo 113-8656, Japan, Department of Clinical Vascular Regeneration, Graduate School of Medicine, The University of Tokyo, 7-3-1 Hongo, Bunkyo-ku, Tokyo 113-8655, Japan, Division of Clinical Biotechnology, Center for Disease Biology and Integrative Medicine, Graduate School of Medicine, The University of Tokyo, 7-3-1 Hongo, Bunkyo-ku, Tokyo 113-0033, Japan, and Center for NanoBio Integration, The University of Tokyo, 7-3-1 Hongo, Bunkyo-ku, Tokyo 113-8656, Japan*

Received January 15, 2008; E-mail: Kataoka@bmw.t.u-tokyo.ac.jp

***Abstract:*** PEG-based polyplex micelles, which can detach the surrounding PEG chains responsive to the intracellular reducing environment, were developed as nonviral gene vectors. A novel block catiomer, PEG-SS-P[Asp(DET)], was designed as follows: (i) insertion of biocleavable disulfide linkage between PEG and polycation segment to trigger PEG detachment and (ii) a cationic segment based on poly(aspartamide) with a flanking *N*-(2-aminoethyl)-2-aminoethyl group, P[Asp(DET)], in which the Asp(DET) unit acts as a buffering moiety inducing endosomal escape with minimal cytotoxicity. The polyplex micelles from PEG-SS-P[Asp(DET)] and plasmid DNA (pDNA) stably dispersed in an aqueous medium with a narrowly distributed size range of ~80 nm due to the formation of hydrophilic PEG palisades while undergoing aggregation by the addition of 10 mM dithiothreitol (DTT) at the stoichiometric charge ratio, indicating the PEG detachment from the micelles through the disulfide cleavage. The PEG-SS-P[Asp(DET)] micelles showed both a 1–3 orders of magnitude higher gene transfection efficiency and a more rapid onset of gene expression than PEG-P[Asp(DET)] micelles without disulfide linkages, due to much more effective endosomal escape based on the PEG detachment in endosome. These findings suggest that the PEG-SS-P[Asp(DET)] micelle may have promising potential as a nonviral gene vector exerting high transfection with regulated timing and minimal cytotoxicity.

## Introduction

Successful gene therapy, which is a promising treatment for numerous intractable diseases, relies on the development of efficient gene vectors. Polyplexes formed by electrostatic interaction between plasmid DNA (pDNA) and cationic polymers (catiomers) have attracted much attention as a safe, versatile alternative to viral vectors.[1–7] A promising approach to realizing the polyplexes for in vivo gene delivery is the use of PEG-based block catiomers. These catiomers spontaneously associate with pDNA to form sub-100 nm polyplex micelles with a dense, hydrophilic PEG palisade surrounding the core.[8–11] These micelles show high colloidal stability under physiological conditions and substantial transfection activity against various cell types even after preincubation with serum proteins.[12,13] Moreover, polyplex micelles demonstrate prolonged blood circulation and in vivo gene transfer to the liver and tumor.[14–16]

[†] Department of Materials Engineering, The University of Tokyo.
[‡] Department of Bioengineering, The University of Tokyo.
[§] Department of Clinical Vascular Regeneration, The University of Tokyo.
[∥] Center for Disease Biology and Integrative Medicine, The University of Tokyo.
[⊥] Center for NanoBio Integration, The University of Tokyo.

(1) Pack, D. W.; Hoffman, A. S.; Pun, S.; Stayton, P. S. *Nat. Rev. Drug Discov.* **2005**, *4*, 581–593.
(2) Merdan, T.; Kopecek, J.; Kissel, T. *Adv. Drug Delivery Rev.* **2002**, *54*, 715–758.
(3) Wagner, E.; Meyer, M. *Hum. Gene Ther.* **2006**, *17*, 1062–1076.
(4) Kabanov, A. V. *Adv. Drug Delivery Rev.* **2006**, *58*, 1597–1621.
(5) Park, T. G.; Jeong, J. H.; Kim, S. W. *Adv. Drug Delivery Rev.* **2006**, *58*, 467–486.
(6) Osada, K.; Kataoka, K. *Adv. Polym. Sci.* **2006**, *202*, 113–153.
(7) Neu, M.; Fischer, D.; Kissel, T. *J. Gene Med.* **2005**, *7*, 992–1009.
(8) Katayose, S.; Kataoka, K. *Bioconjugate Chem.* **1997**, *8*, 702–707.
(9) Katayose, S.; Kataoka, K. *J. Pharm. Sci.* **1998**, *87*, 160–163.
(10) Ogris, M.; Brunner, S.; Schuller, S.; Kircheis, S.; Wagner, E. *Gene Ther.* **1999**, *6*, 595–605.
(11) Kwok, K. Y.; McKenzie, D. L.; Evers, D. L.; Rice, K. G. *J. Pharm. Sci.* **1999**, *88*, 996–1003.
(12) Itaka, K.; Yamauchi, K.; Harada, A.; Nakamura, K.; Kawaguchi, H.; Kataoka, K. *Biomaterials* **2003**, *24*, 4495–4506.
(13) Itaka, K.; Harada, A.; Nakamura, K.; Kawaguchi, H.; Kataoka, K. *Biomacromolecules* **2002**, *3*, 841–845.
(14) Harada-Shiba, M.; Yamauchi, K.; Harada, A.; Takanisawa, I.; Shimokado, K.; Kataoka, K. *Gene Ther.* **2002**, *9*, 407–414.
(15) Miyata, K.; Kakizawa, K.; Nishiyama, N.; Yamasaki, Y.; Watanabe, T.; Kohara, M.; Kataoka, K. *J. Controlled Release* **2005**, *109*, 15–23.

10.1021/ja800336v CCC: $40.75 

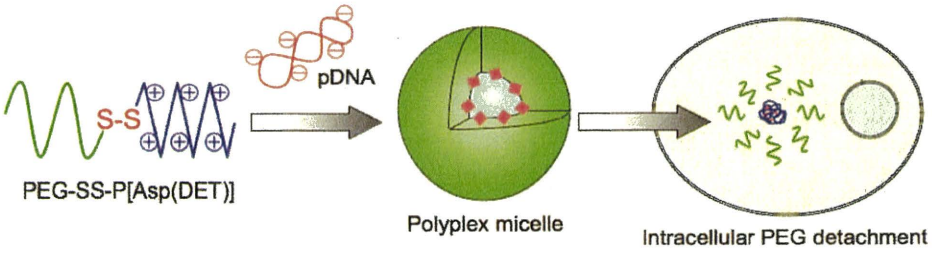


***Figure 1.*** Schematic illustration of PEG-detachable polyplex micelle formation and the PEG detachment in the reducing intracellular environment.

We recently reported high transfection efficiency and low cytotoxicity with the use of polyplex micelles formed by PEG-*block*-poly(aspartamide) copolymers carrying the *N*-(2-aminoethyl)-2-aminoethyl group in the side chain (PEG-P[Asp(DET)]).[17] With regard to in vivo application, the polyplex micelles demonstrate appreciable gene transfer into vascular lesions without any vessel occlusion by thrombus[18] and bone regeneration of a mouse bone defect when transfected with genes coding for osteogenic factors.[19] These successful in vivo gene therapies have been explained by the specific structure of the side chain of P[Asp(DET)], in which the 1,2-ethanediamine moiety of the *N*-(2-aminoethyl)-2-aminoethyl group exhibits a distinct two-step protonation behavior, suggesting a potential proton sponge capacity of Asp(DET) units for efficient endo/lysosomal escape.[17]

However, polyplex micelles formed from PEG-P[Asp(DET)] could be further improved upon to achieve successful in vivo systemic therapies. P[Asp(DET)] homopolymer polyplexes show higher transfection efficiency than PEG-P[Asp(DET)] micelles especially at low charge ratios,[20] suggesting that the PEG palisade surrounding PEG-P[Asp(DET)] polyplex micelles would hamper the transfection. The decrease in gene transfection efficiency by PEGylation to cationers (PEG dilemma) is also observed in previous work.[16,21,22] In addition, the time-dependent monitoring of gene expression against multicellular tumor spheroids reveals that the polyplex micelles from PEG-P[Asp(DET)] cause delayed gene expression, compared with polyplexes from cationic homopolymers.[20] This is sometimes undesired especially when rapid expression is required. On the other hand, the polyplexes from P[Asp(DET)] homocationers tend to aggregate through interactions with serum proteins,[18] suggesting limited in vivo application of the system without PEGylation. Although P[Asp(DET)] homocationers exhibited appreciably lower cytotoxicity compared with typical polycations such as polyethyleneimine (PEI),[23] PEGylation to P[Asp(DET)] further decreases the cytotoxicity to obtain successful transfection of primary cells.[17,18,20]

In order to overcome the aforementioned PEG dilemma, we designed here PEG detachable smart polyplex micelles sensitive to the intracellular environment as a smart gene vector (Figure 1). Block cationers containing disulfide linkages between PEG and P[Asp(DET)] segments, PEG-SS-P[Asp(DET)], were synthesized to obtain this design goal (Scheme 1). Subsequent disulfide reduction of the block cationer can occur during several steps of the endocytic pathway.[24] The cytoplasm and nuclear space are highly reducing environments due to abundant reduced glutathione (GSH) as well as redox enzymes such as the thioredoxin family. In addition, several studies suggest that disulfide bond reduction can begin on the exofacial surface of the cell and must continue after endocytosis. In this regard, involvement of plasma membrane-associated protein disulfide isomerase (PDI) is strongly implicated, as disulfide reduction is inhibited by an anti-PDI antibody and a PDI-inhibitor.[25,26] Moreover, NADH-oxidase (NOX) is reported as another cell surface-associated protein with disulfide−thiol interchange activity similar to PDI. Interestingly, the activity of this enzyme is constitutively activated in cancerous cells such as HeLa and hepatoma cells.[27] Finally, cysteine is actively transported from the cytoplasm to the lysosome lumen via a specific transporter in fibroblasts.[28]

Though the cleavage mechanism of the disulfide linkages cannot be predicted for the PEG-SS-P[Asp(DET)] micelle system utilized herein, the effect of PEG detachment on the gene transfection efficiency can be predicted based on where cleavage may occur. As a result of PEG detachment at the cell surface, the exposed cation segments may trigger a strong association to cells, increasing the cellular uptake of the micelles. Inside endosomes, the PEG detachment would cause the interaction between the exposed cation segments and the endosomal membrane and/or increase endosomal pressure, resulting in the destruction of the endosomal membrane to enable effective endosomal escape. In the cytoplasm and nucleus, the release of pDNA that forms the polyplex core might become smoother because steric repulsion disappears as the PEG cleaves, causing easier access of cellular polyanions to the complex core. Even if the reduction of disulfide linkages occurs in any of the steps outlined above, a more rapid alteration of gene expression and an increased transfection efficiency are expected.

(16) Kursa, M.; Walker, G. F.; Roessler, V.; Ogris, M.; Roedl, W.; Kircheis, R.; Wagner, E. *Bioconjugate Chem.* **2003**, *14*, 222–231.
(17) Kanayama, N.; Fukushima, S.; Nishiyama, N.; Itaka, K.; Jang, W.-D.; Miyata, K.; Yamasaki, Y.; Chung, U.-i.; Kataoka, K. *ChemMedChem* **2006**, *1*, 439–444.
(18) Akagi, D.; Oba, M.; Koyama, H.; Nishiyama, N.; Fukushima, S.; Miyata, T.; Nagawa, H.; Kataoka, K. *Gene Ther.* **2007**, *14*, 1029–1038.
(19) Itaka, K.; Ohba, S.; Miyata, K.; Kawaguchi, H.; Nakamura, K.; Takato, T.; Chung, U.-i.; Kataoka, K. *Mol. Ther.* **2007**, *15*, 1655–1662.
(20) Han, M.; Bae, Y.; Nishiyama, N.; Miyata, K.; Oba, M.; Kataoka, K. *J. Controlled Release* **2007**, *121*, 38–48.
(21) Brissault, B.; Kichler, A.; Leborgne, C.; Danos, O.; Cheradame, H.; Gau, J.; Auvray, L.; Guis, C. *Biomacromolecules* **2006**, *7*, 2863–2870.
(22) Sagara, K.; Kim, S. W. *J. Controlled Release* **2002**, *79*, 271–281.
(23) Masago, K.; Itaka, K.; Nishiyama, N.; Chung, U.-i.; Kataoka, K. *Biomaterials* **2007**, *28*, 5169–5175.
(24) Saito, G.; Swanson, J. A.; Lee, K.-D. *Adv. Drug Delivery Rev.* **2003**, *55*, 199–215.
(25) Feener, E. P.; Shen, W. C.; Ryser, H. J. *J. Biol. Chem.* **1990**, *265*, 18780–18785.
(26) Mandel, R.; Ryser, H. J.; Ghani, F.; Wu, M.; Peak, D. *Proc. Natl. Acad. Sci. U.S.A.* **1993**, *90*, 4112–4116.
(27) Morre, D. J.; Morre, D. M. *Free Radical Res.* **2003**, *37*, 795–808.
(28) Pisoni, R. L.; Acker, T. L.; Lisowski, K. M.; Lemons, R. M.; Thoene, J. G. *J. Cell Biol.* **1990**, *110*, 327–335.

***Scheme 1.*** Synthetic Route of PEG-SS-P[Asp(DET)] Synthesis (Left) and the Chemical Structures of Control Polymers Used in This Experiment (PEG-P[Asp(DET)] and P[Asp(DET)]) (Right)

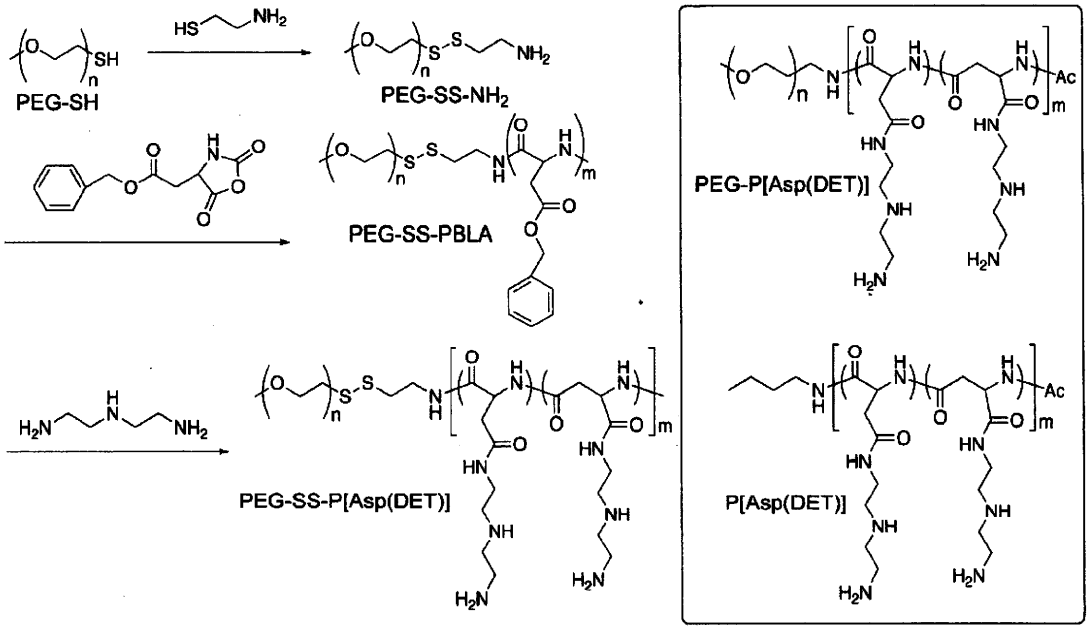


Based on such assumptions, we newly synthesized the PEG-SS-P[Asp(DET)] copolymer and prepared polyplex micelles sensitive to reducing environments. These micelles were expected to show comparable colloidal stability to PEG-P[Asp(DET)] micelles before cellular uptake, while, inside the cell, detachment of PEG would enable pDNA activity and alteration to gene expression. Therefore, careful characterization of both the PEG-SS-P[Asp(DET)] copolymer and the polyplex micelles was performed in regards to the reduction of disulfide linkages. In addition, the influence of the PEG detachment on the onset of gene expression and the mechanism of the disulfide reduction were evaluated through the time-dependent observation of the gene expression and the intracellular localization of pDNA.

## Materials and Methods

**Materials.** α-Methoxy-ω-mercapto PEG (PEG-SH, $M_n = 10000$, $M_w/M_n = 1.03$) and β-benzyl-L-aspartate *N*-carboxyanhydride (BLA-NCA) were obtained from NOF Co. (Tokyo, Japan). Methanol (MeOH), 2-aminoethanethiol, benzene, acetonitrile, hexane, ethyl acetate, and D-luciferin were purchased from Wako Chemical Industries, Ltd. (Osaka, Japan). Dichloromethane, *N*,*N*-dimethylformamide (DMF), diethylenetriamine (DET), and *N*-methyl-2-pyrrolidone (NMP) were also purchased from Wako Chemical Industries and purified by distillation before use. A pGL3 control vector, which was purchased from Promega Co. (Madison, WI), was used as pDNA in all the experiments. This pDNA was amplified in competent DH5α *Escherichia coli* and purified using HiSpeed Plasmid MaxiKit purchased from QIAGEN Inc. (Valencia, CA). Water was purified using a Milli-Q instrument (Millipore, Bedford, MA).

**Synthesis of PEG-SS-P[Asp(DET)].** As shown in Scheme 1, PEG-SH (1 g, 0.1 mmol) was dissolved in MeOH (100 mL), followed by the reaction with 2-aminoethanethiol (100 equiv to PEG-SH, 0.77 g, 10 mmol) at room temperature to obtain PEG-SS-$NH_2$. After a GPC peak due to PEG dimers (PEG-SS-PEG) generated by the side reaction disappeared, the reaction mixture was dialyzed against MeOH for 2 days and evaporated. Then, 80 mL of benzene were added, and the mixture was freeze-dried to obtain the white powder. To remove the PEG disulfide dimers (PEG-SS-PEG) generated during the dialysis, the powder dissolved in 30 mL of $H_2O/CH_3CN$ (4:1) was loaded onto a CM Sephadex C-50 cation exchange chromatograph (GE Healthcare UK, Ltd., Little Chalf-ont, England), eluted with $H_2O/CH_3CN$ (4:1) containing 0.125% $NH_3$. The eluate was evaporated and freeze-dried with distilled water to obtain the PEG-SS-$NH_2$ (570 mg, 57% yield). From gel permeation chromatography (GPC), $M_n$ and $M_w/M_n$ were determined to be 9880 and 1.02, respectively. The conversion to the aminoethanethiol moiety was confirmed to be quantitative (94%) based on the $^1$H NMR data [$CH_3$ (3.2 ppm) and $CH_2$ (2.8 ppm)] (Figure S1) measured with a JEOL EX300 spectrometer (JEOL, Tokyo, Japan).

The PEG-SS-poly(β-benzyl L-aspartate) (PEG-SS-PBLA) copolymer was prepared by the ring opening polymerization of BLA-NCA (4.4 mmol, 1.1 g) in $CH_2Cl_2$/DMF (10:1, 15 mL) at 35 °C from the terminal primary amino group of PEG-SS-$NH_2$ (0.04 mmol, 400 mg).[29] The reaction mixture was precipitated into hexane/AcOEt (6:4). After filtration, the precipitate was dissolved in a small amount of $CH_2Cl_2$, followed by the addition of an excess amount of benzene, and lyophilized to obtain the white powder (910 mg, 61% yield). The degree of polymerization (DP) of PBLA was calculated to be 100 from $^1$H NMR spectroscopy based on the peak intensity of benzyl protons of PBLA side chains (7.3 ppm) to the methylene protons of the PEG chain (3.6 ppm) (Figure S2).

Lyophilized PEG-SS-PBLA (130 mg) was dissolved in NMP (5.2 mL) at 27 °C, followed by the reaction with DET (2.3 mL, 50 equiv to benzyl group of PBLA segment) diluted in NMP (2.3 mL) under anhydrous conditions at 15 °C. After 15 min, the reaction mixture was slowly added dropwise into an aqueous solution of acetic acid (10% v/v, 40 mL) and dialyzed against a solution of 0.01 N HCl and, subsequently, distilled water (MWCO: 6–8000 Da). The final solution was lyophilized to obtain the polymer as the chloride salt form with a yield of 66% (104 mg). The structure of this block cationer was confirmed by $^1$H NMR and size-exclusion chromatography (SEC) [column: Superdex 200 10/300 GL (GE Healthcare UK, Ltd.); eluent: 10 mM Tris-HCl buffer + 500 mM NaCl (pH 7.4); flow rate: 0.75 mL/min; detector RI; ambient temperature].

(29) Harada, A.; Kataoka, K. *Macromolecules* **1995**, *28*, 5294–5299.

**Preparation of PEG-SS-P[Asp(DET)]/pDNA Polyplex Micelles.** The PEG-SS-P[Asp(DET)] block copolymer and pDNA were separately dissolved in 10 mM Tris-HCl buffer (pH 7.4). The polymer solution was added to a 2-times-excess volume of 50 $\mu$g/mL pDNA solution to form the polyplex micelles at various *N/P*, the residual molar ratio of the amino group in the block catiomer to phosphate group in pDNA. The final concentration of pDNA in all the samples was adjusted to 33 $\mu$g/mL. The PEG-P[Asp(DET)] block copolymer ($M_w$ = 39 000; DP of P[Asp(DET)] segment: 100) and P[Asp(DET)] (DP = 98) (Scheme 1) were used as controls, and their polyplexes were prepared in the same way as PEG-SS-P[Asp(DET)]/pDNA polyplex micelles.

**Gel Retardation Assay.** Polyplex solutions formed with pDNA (33 $\mu$g/mL) were diluted to 20 $\mu$g/mL with 10 mM Tris-HCl buffer and then electrophoresed at 100 V for 1 h on a 0.9 wt% agarose gel in 3.3 mM Tris-acetic acid buffer containing 1.7 mM sodium acetate. The migrated pDNA was visualized with ethidium bromide staining (0.5 $\mu$g/mL in deionized water).

**Dynamic Light Scattering (DLS) Measurements.** The size of the polyplexes was evaluated by DLS. Sample solutions with various *N/P* ratios in 10 mM Tris-HCl buffer (pH 7.4) were adjusted to have a pDNA concentration of 33 $\mu$g/mL. DLS measurements were carried out at 37 °C using a Zetasizer Nano-ZS instrument (Malvern Instruments, Malvern, UK), equipped with a He−Ne ion laser ($\lambda$ = 633 nm) with a scattering angle of 90°.

**Radiolabeling of pDNA and Cellular Uptake Study of the Polyplexes.** pDNA was radioactively labeled with $^{32}$P-dCTP using the Nick Translation System (Invitrogen Co., Carlsbad, CA). Unincorporated nucleotides were removed using the High Pure PCR Product Purification Kit (Roche Diagnostics Co., Indianapolis, IN). After the purification, 7 $\mu$g of labeled pDNA were mixed with 700 $\mu$g of nonlabeled pDNA. The polyplex and micelle samples were prepared by mixing the radioactive pDNA solution with each polymer solution (33 $\mu$g pDNA/mL). For the cellular uptake experiment, HeLa cells were seeded in Dulbecco's modified Eagle medium (DMEM) containing 10% fetal bovine serum (FBS) on 24-well tissue culture treated plates 24 h prior to experimentation. The cells were incubated with 30 $\mu$L of the radioactive polyplex solution (1 $\mu$g of pDNA/well) in 400 $\mu$L of DMEM containing 10% FBS. After 6 h of incubation, the cells were washed 3 times with PBS and lysed with 200 $\mu$L of cell culture lysis buffer (Promega, Co., Madison, WI). The lysates were mixed with 5 mL of scintillation cocktail, Ultima Gold (PerkinElmer, MA), and then, the radioactivity was measured using a liquid scintillation counter. The results are presented as a mean and standard deviation of the mean obtained from four samples.

**In Vitro Transfection.** HeLa cells were seeded on 24-well culture plates and incubated for 24 h in 400 $\mu$L of DMEM containing 10% FBS before transfection. The cells were then incubated with the polyplex micelles prepared from PEG-SS-P[Asp(DET)], PEG-P[Asp(DET)], and P[Asp(DET)] (30 $\mu$L, 1 $\mu$g of pDNA/well) with various *N/P* ratios in DMEM containing 10% FBS for 6 h, followed by an additional incubation for 42 h in the absence of polyplexes. The cells were washed in triplicate with 200 $\mu$L of Dulbecco's PBS and lysed by the addition of 400 $\mu$L/well of the Promega lysis buffer. Luciferase gene expression was evaluated using the Luciferase Assay System (Promega Co., Madison, WI) and a Lumat LB957 luminometer (Berthold Technologies Co., Bad Wildbad, Germany). The results were expressed as light units per milligram of cell protein determined by a BCA assay kit (PIERCE Biotechnology, Rockford, IL). The results are presented as a mean and standard deviation of the mean obtained from four samples.

**Time-Dependent Monitoring of in Vitro Transfection.** HeLa cells and 293T cells were seeded on 35-mm culture dishes and incubated for 24 h in 2 mL of DMEM containing 10% FBS before transfection. The cells were then incubated with the polyplex micelles prepared from PEG-SS-P[Asp(DET)], PEG-P[Asp(DET)], and P[Asp(DET)] (90 $\mu$L/dish, 3 $\mu$g of pDNA/dish) at *N/P* = 32 in DMEM containing 10% FBS. After 6 h, the medium was exchanged with fresh media containing 100 $\mu$M D-luciferin. The dishes were set in a luminometer incorporated in a small $CO_2$ incubator (AB-2550 Kronos Dio, ATTO Co., Tokyo, Japan), and the bioluminescence was monitored every 20 min (2 min collection time).

**Confocal Laser Scanning Microscope (CLSM) Observation.** pDNA was labeled with Cy5 using the Label IT Nucleic Acid Labeling Kit (Mirus, Madison, WI) according to the manufacture's protocol. HeLa cells were seeded on a 35-mm glass base dish (Iwaki, Japan) and incubated overnight in 1 mL of DMEM containing 10% FBS. After the medium was replaced with fresh medium, 90 $\mu$L of polyplex solution containing 3 $\mu$g of Cy5-labeled pDNA (*N/P* = 32) were applied. After 6 h of incubation, the medium was removed, the cells were washed twice with PBS, and fresh media was added. The intracellular distributions of the polyplex micelles were observed by CLSM following acidic late endosome and lysosome staining with LysoTracker Green (Molecular Probes, Eugene, OR). The CLSM observation was performed using LSM 510 (Carl Zeiss, Germany) with a 63× objective (C-Apochromat, Carl Zeiss, Germany) at excitation wavelengths of 488 nm (Ar laser) and 633 nm (He−Ne laser) for LysoTracker Green and Cy5, respectively. Colocalization of polyplex micelles in the late endosome and lysosome was quantified as follows:

Colocalization ratio = Cy5 pixels colocalization/Cy5 pixels total

where Cy5 pixels colocalization represents the number of pixels with Cy5 colocalizing with LysoTracker inside the cells and the Cy5 pixels total represents number of all pixels with Cy5 existing in the cells. The results are presented as a mean and standard error of the mean obtained from 10 cells.

## Results and Discussion

**Synthesis of PEG-SS-P[Asp(DET)].** A PEG-poly(aspartamide) block copolymer with a disulfide linkage between PEG and poly(aspartamide) was prepared as shown in Scheme 1. Initially, α-methoxy-ω-mercapto PEG (PEG-SH, $M_n$ = 10 000) was reacted with 2-aminothanethiol in MeOH to introduce a primary amino group into PEG-SH via a disulfide linkage. The conversion ratio was confirmed to be 94% based on the $^1$H NMR data (Figure S1). Then, β-benzyl L-aspartate *N*-carboxyanhydride (BLA-NCA) was polymerized in $CH_2Cl_2$/DMF at 35 °C by an initiation from the terminal primary amino group of PEG-SS-$NH_2$. The degree of polymerization (DP) of PBLA was calculated to be 100 from $^1$H NMR spectroscopy, and GPC measurement revealed that the obtained PEG-SS-PBLA showed a unimodal molecular weight distribution (Figure S2). The aminolysis of PEG-SS-PBLA in NMP in the presence of a molar excess of diethylenetriamine (DET, 50 equiv relative to benzyl groups) was carried out. The $^1$H NMR spectrum of the obtained polymer (Figure S3) reveals that the introduction of DET into the side chains of PBLA was almost quantitative (98.5%) in spite of the extremely short reaction time (15 min) and relatively low temperature (15 °C). The detailed mechanism of this unique aminolysis reaction of PBLA was reported elsewhere.[30] Size-exclusion chromatography (SEC) measurements revealed a unimodal molecular weight distribution of the obtained polymer (Figure 2, line 1), suggesting a minimal occurrence of inter- or intrapolymer cross-linking by DET during aminolysis. To confirm the presence of disulfide linkages between PEG and polycation segments, SEC measurement was done after the addition of 10 mM dithiothreitol (DTT) to the PEG-SS-P[Asp(DET)] solution. In the SEC chromatogram, two overlapping peaks (Figure 2, line 2) were observed at elution times extremely similar to those for PEG-SH (Figure 2, line 3) and

(30) Nakanishi, M.; Park, J.-S.; Jang, W.-D.; Oba, M.; Kataoka, K. *React. Funct. Polym.* **2007**, *67*, 1361–1372.

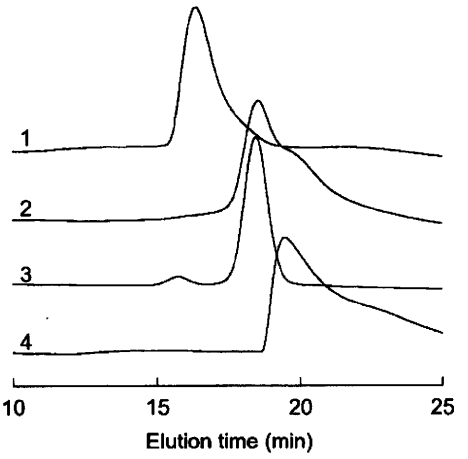


***Figure 2.*** SEC charts of PEG-SS-P[Asp(DET)] (line 1), PEG-SS-P[Asp(DET)] after 4 h incubation with 10 mM DTT (line 2), PEG-SH (line 3), and P[Asp(DET)] (line 4).

P[Asp(DET)] (Figure 2, line 4), indicating that the obtained polymer was linked via a disulfide linkage between PEG and P[Asp(DET)] segments.

**Formation of Polyplex Micelles from pDNA and PEG-SS-P[Asp(DET)].** Polyplex micelles were prepared by mixing each polymer solution with the pDNA solution at various *N/P* ratios. In order to demonstrate polyplex formation between PEG-SS-P[Asp(DET)] and pDNA, a gel electrophoresis retardation assay was performed using 0.9 wt % agarose gel. A PEG-P[Asp(DET)] block copolymer without the disulfide linkage and P[Asp(DET)] homocatiomer were used as controls (Scheme 1). As shown in Figure 3, the band of free pDNA disappeared at *N/P* > 2 in all of the samples, indicating successful and complete polyplex formation between pDNA and the three catiomers. This is stoichiometrically consistent with the monoprotonated form of the ethylenediamine unit in PEG-P[Asp(DET)] and P[Asp(DET)] at pH 7.4.[17,20] The diameters of the polyplexes or the polyplex micelles prepared at different *N/P* ratios are shown in Figure 4a. The diameters of the polyplex micelles from PEG-P[Asp(DET)] and PEG-SS-P[Asp(DET)] were determined to be 80–90 nm throughout the examined *N/P* ratios (1–16). On the other hand, the polyplexes from P[Asp(DET)] formed large aggregates with a size of approximately 600 nm specifically at *N/P* ~2. Considering that zeta-potential of the P[Asp(DET)] polyplex was close to neutral at *N/P* = 2 (Figure S4), the aggregation was presumably due to the formation of charge stoichiometric complexes showing lower electrostatic repulsion among the polyplexes. The system of PEG-SS-P[Asp(DET)] and PEG-P[Asp(DET)] did not show such aggregation, indicating a high colloidal stability due to the steric repulsion of the PEG palisades of the shell.[31]

**Reducing Environment-Sensitive Cleavage of the Disulfide Linkages of the Polyplex Micelles from PEG-SS-P[Asp(DET)].** To confirm the detachment of PEG from the PEG-SS-P[Asp(DET)] polyplex micelles, the diameter of the micelles (*N/P* = 2) was monitored after the addition of 10 mM DTT, as a model reaction for the reducing environment of the cytoplasm. As shown in Figure 4b, 10 mM DTT rapidly induced an increase in size of PEG-SS-P[Asp(DET)] micelles, whereas, in the case of control

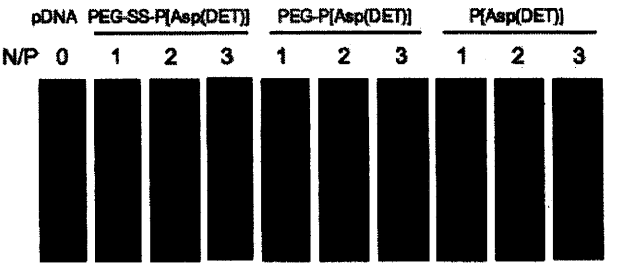


***Figure 3.*** Gel retardation assay of the polyplexes.

micelles from PEG-P[Asp(DET)], such a size increase was not observed, indicating that the PEG chains on the PEG-SS-P[Asp(DET)] micelles were detached due to the cleavage of the disulfide bond. Moreover, as a model of the extracellular environment, the polyplex micelles were incubated in 10 $\mu$M DTT, which is an effective 50-fold molar equivalent of the PEG-SS-P[Asp(DET)] within the micelles. As a result, the polyplex micelles did not show increased size (Figure 4b), indicating that the PEG detachment would be dependent on the concentration of the surrounding thiol groups. To check the PEG detachment at other *N/P* ratios, the $\zeta$-potential of the polyplex micelles was measured in the absence or presence of 10 mM DTT. The polyplexes from PEG-SS-P[Asp(DET)] and PEG-P[Asp(DET)] were observed to have $\zeta$-potentials with a very small absolute value (~4 mV) in *N/P* > 2 (Figure S4), suggesting that the polyplexes from the PEG-*b*-catiomers form a core–shell micellar architecture with a hydrophilic and neutral PEG shell surrounding the polyplex core. After the addition of 10 mM DTT, the $\zeta$-potential of PEG-SS-P[Asp(DET)] polyplex micelles shifted to a positive value (~28 mV) comparable to that of the P[Asp(DET)] polyplexes. On the other hand, there was no change in the $\zeta$-potential of PEG-P[Asp(DET)] micelles by the addition of DTT. These results indicate that, regardless of *N/P* ratio, the surface-covered PEG chains detached from the PEG-SS-P[Asp(DET)] polyplex micelles when present in a reducing environment.

**Cellular Uptake Study.** Though the PEG-SS-P[Asp(DET)] polyplex micelles were responsive to reducing environments, it is significant to determine where the PEG chains will be detached after contact with cells. Rice et al. concluded that the complexes formed from PEG(5 kDa)-SS-$Lys_{18}$ and pDNA showed more in vitro cellular uptake than PEG-$Lys_{18}$ complexes without disulfide linkages, suggesting partial reduction of the disulfide linkages outside cells.[32] To confirm that the disulfide linkages were cleaved either outside or inside cells, polyplexes with $^{32}$P-radiolabeled pDNA were prepared and the uptake to human cervical carcinoma HeLa cells was measured. As shown in Figure 5, PEG-SS-P[Asp(DET)] and PEG-P[Asp(DET)] polyplex micelles showed a minimal uptake into the cells, with only ~0.5% of the total dose being taken up. In contrast, 2−4% of P[Asp(DET)] polyplexes were taken into the cells, probably due to the electrostatic association between the positive charge of the polyplexes and the negative charge of the plasma membrane. If the disulfide linkages were reduced prior to uptake by cells, a higher percentage of the PEG-SS-P[Asp(DET)] micelles would be taken up than the PEG-P[Asp(DET)] micelles. In contrast, the cellular uptakes of PEG-P[Asp(DET)] and PEG-SS-P[Asp(DET)] micelles are equivalent, suggesting that the

(31) Kataoka, K.; Harada, A.; Nagasaki, Y. *Adv. Drug Delivery Rev.* **2001**, *47*, 113–131.

(32) Kwok, K. Y.; McKenzie, D. L.; Evers, D. L.; Rice, K. G. *J. Pharm. Sci.* **1999**, *88*, 996–1003.

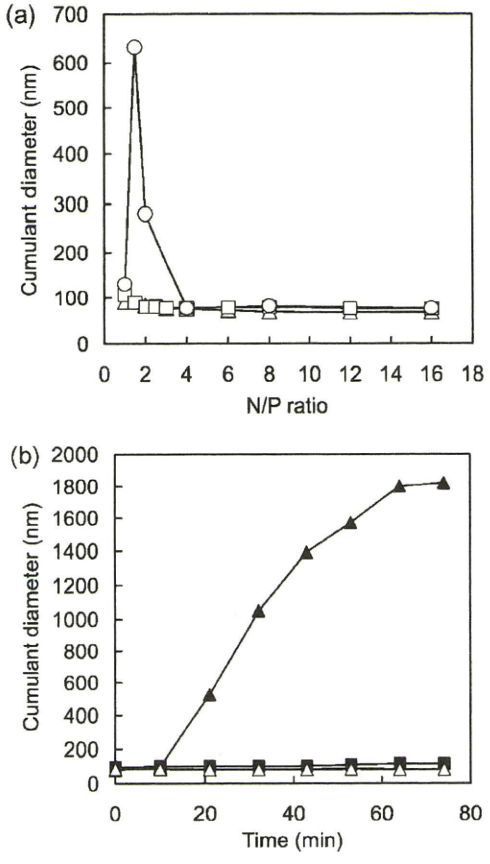


***Figure 4.*** (a) Size of the polyplexes from PEG-SS-P[Asp(DET)] (△), PEG-P[Asp(DET)] (□), and P[Asp(DET)] (○). (b) Time-dependent change of the size of PEG-SS-P[Asp(DET)] polyplex micelles at $N/P = 2$ with 10 mM DTT (▲) and with 10 $\mu$M DTT (△), and PEG-P[Asp(DET)] polyplex micelles with 10 mM DTT (■).

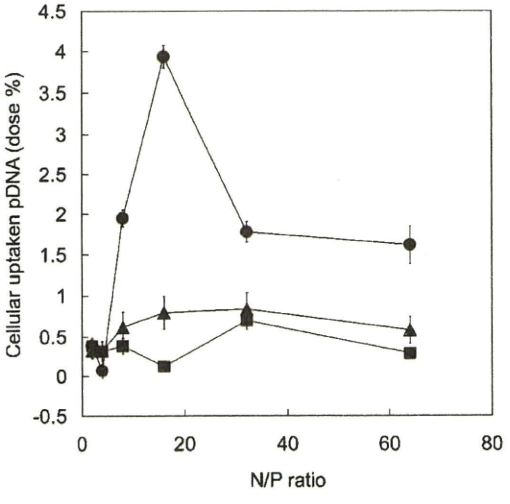


***Figure 5.*** Cellular uptake of pDNA complexed with catiomers; PEG-SS-P[Asp(DET)] (▲), PEG-P[Asp(DET)] (■), and P[Asp(DET)] (●). $^{32}$P-labeled pDNA polyplexes were incubated with HeLa cells in DMEM containing 10% FBS at 37 °C for 6 h. The amount of internalized pDNA is represented as a percentage for the dosed pDNA (1 $\mu$g/well).

PEG-SS-P[Asp(DET)] micelles maintain their PEG palisade structure under normal culture conditions for at least 6 h. Note

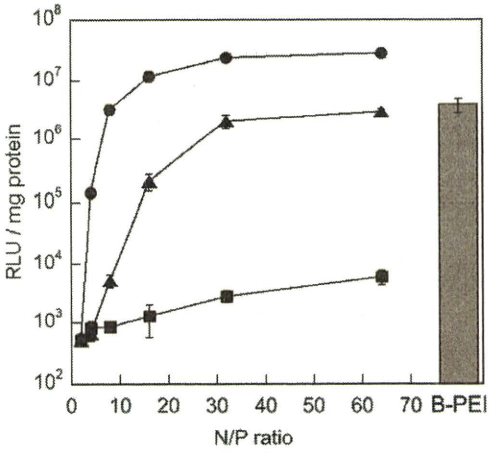


***Figure 6.*** In vitro transfection of the luciferase gene into HeLa cells by polyplexes from PEG-SS-P[Asp(DET)] (▲), PEG-P[Asp(DET)] (■), and P[Asp(DET)] (●) with varying $N/P$ ratios. Branched polyethyleneimine (B-PEI, 25 kDa) at $N/P = 32$ was shown as a control (gray bar). The cells were incubated with each polyplex in DMEM containing 10% FBS for 6 h, followed by incubation for a further 42 h in the absence of the polyplexes. Transfection is reported in relative light units (RLU) per mg of protein.

that there is a decrease in cellular uptake of the P[Asp(DET)] polyplexes with $N/P \geq 32$. This may be due to inhibition of uptake by free catiomers which are not associated with the polyplexes.

**In Vitro Transfection Efficiency and Cytotoxicity.** The in vitro transfection efficiency of these polyplexes with HeLa cells was assessed using a luciferase assay. Based on the cellular uptake study, cells were incubated with the polyplexes for 6 h, followed by a 42 h incubation after medium replacement. As shown in Figure 6, PEG-SS-P[Asp(DET)] polyplex micelles showed 2–3 orders of magnitude higher transfection efficiency than the PEG-P[Asp(DET)] polyplex micelles at $N/P \geq 16$, which is comparable to branched polyethyleneimine (B-PEI, 25 kDa). It is surprising that the introduction of disulfide linkages to the block catiomers remarkably increased the transfection efficiency, though the efficiency was somewhat less than P[Asp(DET)] polyplexes. Low cytotoxicity together with high transfection efficiency is an extremely important aspect for nonviral gene vectors. The cytotoxicity of the polyplexes was evaluated with the same cell culture procedure as the transfection, followed by the CellTiter-Glo luminescent cell viability assay. Polyplex micelles from PEG-SS-P[Asp(DET)], PEG-P[Asp(DET)], and P[Asp(DET)] polyplexes showed more than 90% cell viability in all $N/P$ ratios tested in this study, while B-PEI polyplexes induced a significant decrease in cell viability (~40%) at $N/P = 64$ (Figure S5). A similar tendency was observed at lower $N/P$ as well in the case of longer incubation times and higher doses (data not shown). These results indicate that P[Asp(DET)] and the block catiomers would be desirable as in vivo gene vectors due to their high transfection efficiency as well as low toxicity.

**Mechanism of the High Transfection Efficiency of PEG-SS-P[Asp(DET)] Micelles.** It is important to understand where the disulfide linkages of the PEG-SS-P[Asp(DET)] polyplex micelles are cleaved inside the cell. Therefore, the time-dependent profile of transfection efficiency was monitored with AB-2550 Kronos Dio (ATTO Co. Ltd., Tokyo, Japan), which is a luminometer incorporated into a small $CO_2$ incubator, allowing continuous measurement of bioluminescence by transfected

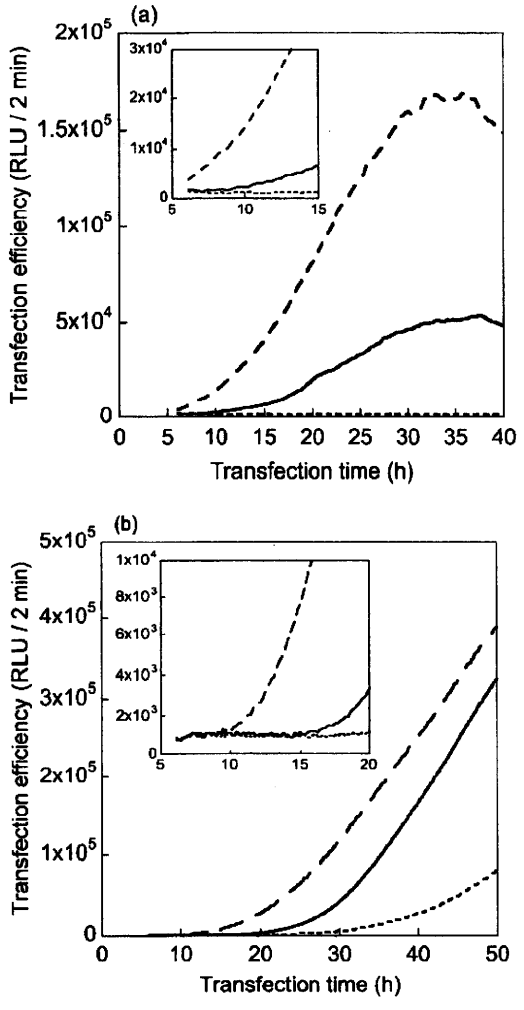


***Figure 7.*** Time-dependent profiles of transfection efficiency against HeLa cells (a) and 293T cells (b) induced by PEG-SS-P[Asp(DET)] (solid line), PEG-P[Asp(DET)] (dotted line), and P[Asp(DET)] (dashed line) polyplexes at $N/P = 32$. The cells were incubated with each polyplex in DMEM containing 10% FBS for 6 h, followed by incubation in DMEM containing 10% FBS and 100 $\mu$M D-luciferin in the absence of polyplexes. The time shown in the $x$-axis started from the addition of polyplex solutions and the measurement started from 6 h. The inserts are expanded figures from 5 to 15 h (a) and from 5 to 20 h (b).

cells. After HeLa cells were incubated with the polyplexes for 6 h, the medium modified to include luciferin was used to culture the cells and bioluminescence from expressed luciferase was monitored at 20 min intervals. As shown in Figure 7a, the gene expression induced by P[Asp(DET)] polyplexes started to be observed immediately after the medium replacement (at 6 h), while the expression by PEG-SS-P[Asp(DET)] micelles started at 11 h and increased remarkably after 16 h. A similar tendency of delayed expression with PEG-SS-P[Asp(DET)] micelle carriers compared with P[Asp(DET)] polyplexes was observed with 293T cells as well (Figure 7b). The reason of the delayed expression of PEG-SS-P[Asp(DET)] micelles is presumably related to the process of the disulfide reduction inside the cell. In addition, clear expression by PEG-SS-P[Asp(DET)] micelles in 293T cells was observed 10 h earlier than PEG-P[Asp(DET)] micelles, probably due to the detachment of PEG chains. These results indicate that PEG-SS-P[Asp(DET)] micelles could regulate the onset of the gene expression, which is a significantly attractive characteristic in this system.

In order to gain more insight into the relationship between the cleavage of disulfide linkages and transfection efficiency, intracellular trafficking of pDNA in the micelles was observed with a confocal laser scanning microscope (CLSM), using PEG-SS-P[Asp(DET)] polyplex micelles with Cy5-labeled pDNA (red) at $N/P = 32$. LysoTracker (green) was used as an endo/lysosomal marker. As shown in Figure 8a, Cy5-pDNA of the polyplex micelles from PEG-P[Asp(DET)] and PEG-SS-P[Asp(DET)] associates to the plasma membrane 6 h after transfection, whereas the red fluorescence from P[Asp(DET)] polyplexes seemed to spread out from the green fluorescence of LysoTracker even at 6 h, indicating fast endosomal escape. This result would correspond to the transfection profile (Figure 7a) where transfection by P[Asp(DET)] polyplexes is observed starting at 6 h. Figure 8b shows CLSM images after 6 h of incubation with the polyplex and 6 h postincubation in the absence of polyplexes, corresponding to the time when a gene expression by PEG-SS-P[Asp(DET)] micelles started (12 h in Figure 7a). In these images, the pDNA of PEG-P[Asp(DET)] micelles is colocalized and sequestered in the endo/lysosome, resulting in the absence of expression in Figure 7a. On the other hand, the pDNA of PEG-SS-P[Asp(DET)] micelles spread out from LysoTracker, indicating that the PEG-SS-P[Asp(DET)] micelles that escaped from the endosome would be capable of inducing gene expression. In the case of P[Asp(DET)] polyplexes, pDNA spread out from endo/lysosome increased remarkably. Time-dependent colocalization of pDNA in the endo/lysosomes was quantified and is shown in Figure 8c. PEG-P[Asp(DET)] micelles exhibited high colocalization even after 2 days, while less colocalization was observed in the PEG-SS-P[Asp(DET)] system, suggesting a more effective endosomal escape. A similar localization profile of pDNA in the PEG-SS-P[Asp(DET)] system was observed in 293T cells (Figure S6). Considering the transfection profile as well as CLMS images (Figure 7 and 8), it is likely that cleavage of the disulfide linkages of PEG-SS-P[Asp(DET)] micelles occurs in the endocytic pathway, resulting in effective endosomal escape probably due to interaction between the exposed polycation segments and endosomal membrane, and/or increased osmotic pressure in the endosome induced by detached PEG chains. As a result, the gene expression onset of PEG-SS-P[Asp(DET)] micelles was intermediate when compared with P[Asp(DET)] polyplexes and PEG-P[Asp(DET)] micelles. There is an issue that disulfide reduction in the endosome would be disfavored due to the low GSH concentration as well as the acidic environment inducing protonation of thiol groups and decreased reactivity of thiol–disulfide oxidoreductase (e.g., PDI, thioredoxin, etc.) because these enzymes typically exhibit optimal activity around neutral pH. Nevertheless, Low et al. directly observed images of disulfide cleavage with FRET technology using folate–SS–rhodamine conjugates.[33] In addition, calcein-loaded polymersome formed from a PEG-SS-poly(propylene sulfide) block copolymer showed the rapid release of calcein inside the endosome due to the disulfide reduction, facilitating endosomal rupture.[34] In the case of the PEG-SS-P[Asp(DET)] system, considering the increased endosomal escape, not all PEG chains but a substantial fraction of them are assumed to be detached

(33) Yang, J.; Chen, H.; Vlahov, I. R.; Cheng, J.-X.; Low, P. S. *Proc. Natl. Acad. Sci. U.S.A.* **2006**, *103*, 13872–13877.
(34) Cerritelli, S.; Velluto, D.; Hubbell, J. A. *Biomacromolecules* **2007**, *8*, 1966–1972.

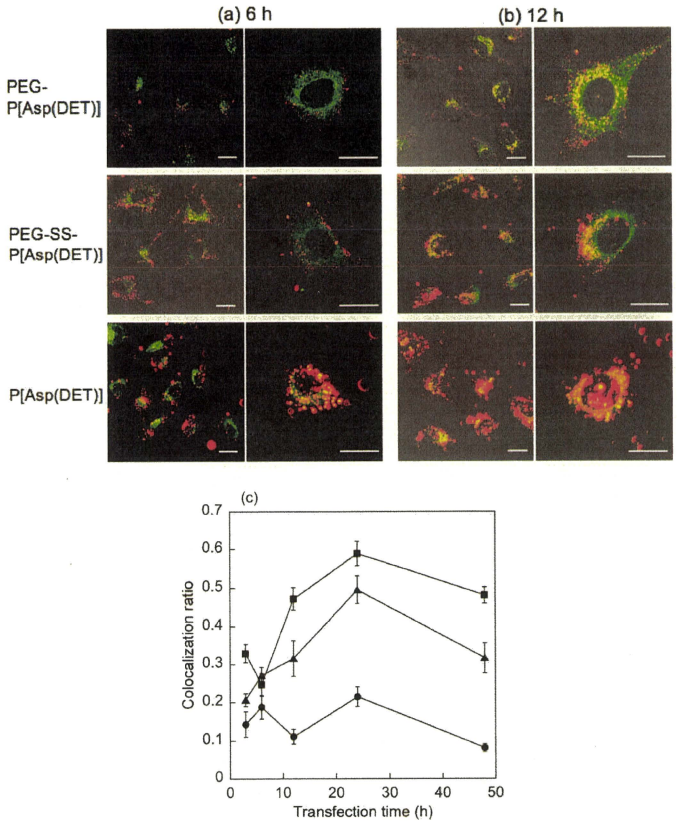


***Figure 8.*** (a, b) Intracellular distribution of pDNA challenged by PEG-P[Asp(DET)] and PEG-SS-P[Asp(DET)] micelles, and P[Asp(DET)] polyplexes at $N/P = 32$. The complexes loaded with Cy5-labeled pDNA (red) were incubated with HeLa cells for 6 h, followed by incubation in the absence of polyplexes. The CLSM observation was performed 6 h (a) and 12 h (b) after transfection, using a 63× objective. The acidic late endosome and lysosome were stained with LysoTracker Green (green). The scale bar represents 20 $\mu$m. (c) Quantitative results of colocalization profile of Cy5-labeled pDNA in late endosome and lysosome transfected by PEG-P[Asp(DET)] (■), PEG-SS-P[Asp(DET)] (▲), and P[Asp(DET)] (●) polyplexes.

in the endocytic pathway as a result of disulfide reduction. In the future, further mechanistic investigations of the disulfide cleavage will be performed to reveal a detailed relationship between PEG detachment and gene transfection efficiency, contributing to establishing the design criteria for smart polyplex micelles useful for in vivo transfection studies.

## Conclusion

We newly synthesized a disulfide-linked block catiomer, PEG-SS-P[Asp(DET)], to develop a PEG detachable polyplex micelle sensitive to an intracellular reducing environment. This micelle showed several orders of magnitude higher gene transfection efficiency than a micelle without disulfide linkages in spite of the similar level of their cellular uptakes. Moreover, gene expression induced by the PEG-SS-P[Asp(DET)] micelle started between the expression onsets of the P[Asp(DET)] polyplex and PEG-P[Asp(DET)] micelle, indicating that the PEG-SS-P[Asp(DET)] micelle could regulate the onset of the gene expression. CLSM images revealed that this transfection behavior of the PEG-SS-P[Asp(DET)] micelle could be explained by effective endosomal escape due to the PEG detachment in the endosome. As this micelle overcame the PEG dilemma, it would be highly promising for in vivo application to exert spatio-temporal regulated transfection with minimal cytotoxicity.

# Comparison of the effects of the kinase inhibitors imatinib, sorafenib, and transforming growth factor-β receptor inhibitor on extravasation of nanoparticles from neovasculature

Mitsunobu R. Kano,[1,2,3,4] Yukari Komuta,[1,5] Caname Iwata,[1] Masako Oka,[1] Yo-taro Shirai,[1] Yasuyuki Morishita,[1] Yasuyoshi Ouchi,[4] Kazunori Kataoka[2] and Kohei Miyazono[1,2,6]

[1]Department of Molecular Pathology, Graduate School of Medicine, University of Tokyo, 7-3-1 Hongo, Bunkyo-ku, Tokyo, 113-0033; [2]Center for Nano-Bio Integration, University of Tokyo, Tokyo, 113-8656; [3]Medical Scientist Training Program, Faculty of Medicine, University of Tokyo, Tokyo, 113-0033; [4]Department of Geriatrics, Graduate School of Medicine, University of Tokyo, 7-3-1 Hongo, Bunkyo-ku, Tokyo, 113-0033; [5]Japan Association for the Advancement of Medical Equipment, 3-42-6 Hongo, Bunkyo-ku, Tokyo, 113-0033, Japan

(Received May 20, 2008/Revised September 11, 2008/Accepted September 14, 2008/Online publication November 25, 2008)

**There are a number of kinase inhibitors that regulate components of the neovasculature. We previously reported the use of transforming growth factor (TGF)-β inhibitor on neovasculature in stroma-rich tumor models to increase the intratumoral distribution of nanoparticles. Here, we compared the effects of two other kinase inhibitors, imatinib and sorafenib, with TGF-β inhibitor (LY364947) on extravasation of a modeled nanoparticle, 2 MDa dextran. We first used a mouse model of neoangiogenesis, the Matrigel plug assay, to compare neovasculature formed inside of and around Matrigel plugs (intraplug and periplug regions, respectively). Intraplug vasculature was more strongly pericyte covered, whereas periplug vasculature was less covered. In this model, TGF-β inhibitor exhibited the most potent effect on intraplug vasculature in increasing the extravasation of dextran, whereas sorafenib had the strongest effect on periplug vasculature. Although imatinib and TGF-β inhibitor each reduced pericyte coverage, imatinib also reduced the density of endothelium, resulting in a decrease in overall delivery of nanoparticles. These findings were confirmed in two tumor models, the CT26 colon cancer model and the BxPC3 pancreatic cancer model. The vasculature phenotype in the CT26 model resembled that in the periplug region, whereas the latter resembled that in the intraplug region. Consistent with this, sorafenib most potently enhanced the accumulation of nanoparticles in the CT26 model, whereas TGF-β inhibitor did in the BxPC3 model. In conclusion, the appropriate strategy for optimization of tumor vasculature for nanoparticles may differ depending on tumor type, and in particular on the degree of pericyte coverage around the vasculature. (*Cancer Sci* 2009; 100: 173–180)**

The effectiveness of drug delivery into tumor tissues is an important issue in the treatment of solid tumors, in addition to the efficacy of drugs in treating tumor cells. For example, gemcitabine, a first-line anticancer agent for pancreatic adenocarcinoma, exhibited potent *in vitro* growth-inhibitory effects on a cultured cell line derived from the human pancreatic adenocarcinoma line BxPC3.[1] However, it exhibited only slight inhibitory effects on xenografted BxPC3 tumors in mice[2] and slight elongation of survival time in tumor-bearing patients, with significant effects only in the improvement of quality of life index in clinical trials.[3]

Many factors might potentially explain this discrepancy, particularly those related to tumor stroma.[4] Among them, tumor vasculature plays an important role in the delivery of anticancer agents. Extravasation of drugs to tumor tissue constitutes an essential part of drug delivery to tumor tissues,[5] whereas the molecular size of compounds is another important determinant of accumulation.[6] We have recently shown that increased leakiness in tumor neovasculature improves the accumulation of nanoparticles in tumor tissues in animal models of pancreatic adenocarcinoma and diffuse-type advanced gastric cancer.[7] In that study, inhibition of transforming growth factor (TGF)-β signaling reduced pericyte coverage and slightly increased endothelial area, resulting in an increase in vascular leakiness without loss of blood flow. However, numerous studies of tumor neovasculature have shown that it is leaky by nature, and that manipulation of vessels to make them less leaky, or induction of vascular normalization, may therefore benefit drug delivery to tumor tissues.[8] This theory has been supported with the use of vascular endothelial growth factor (VEGF) inhibitors. There are a number of VEGF inhibitors available, including neutralizing anti-VEGF antibodies such as bevacizumab (Avastin) and sorafenib (Nexavar). Sorafenib is a small molecular-weight (SMW) compound inhibiting multiple tyrosine kinases, including VEGF receptor (VEGFR) 2.[9]

The roles of pericytes in neoangiogenesis have also been well investigated.[10] Coverage of the neovasculature by pericytes stabilizes vascular structure.[11] Genetic ablation of platelet-derived growth factor (PDGF)-B signaling, one of the major signaling pathways in induction of pericyte maturation and recruitment to the endothelium, results in a bleeding tendency of the neovasculature.[11–13] PDGF-B signaling can be inhibited by the SMW inhibitor (SMWI) imatinib (Gleevec or Glivec), which inhibits the receptor for PDGF-B signaling, PDGF receptor (PDGFR) β, as well as PDGFRα and c-kit.[14] The use of imatinib along with VEGF inhibitors was shown to be effective in inhibiting tumor neovascularization in an animal model of spontaneous pancreatic islet tumor, the RIP-Tag model, through disruption of both pericytes and endothelium.[15]

Here we investigated the changes in vascular leakiness induced by three of the SMWI mentioned above, TGF-β inhibitor (LY364947), sorafenib, and imatinib, in the Matrigel plug assay as well as two animal cancer models. The Matrigel plug assay was carried out by mixing BD Matrigel Basement Membrane Matrix with VEGF-A, fibroblast growth factor (FGF)-2, and

[6]To whom correspondence should be addressed. E-mail: miyazono-ind@umin.ac.jp

doi: 10.1111/j.1349-7006.2008.01003.x

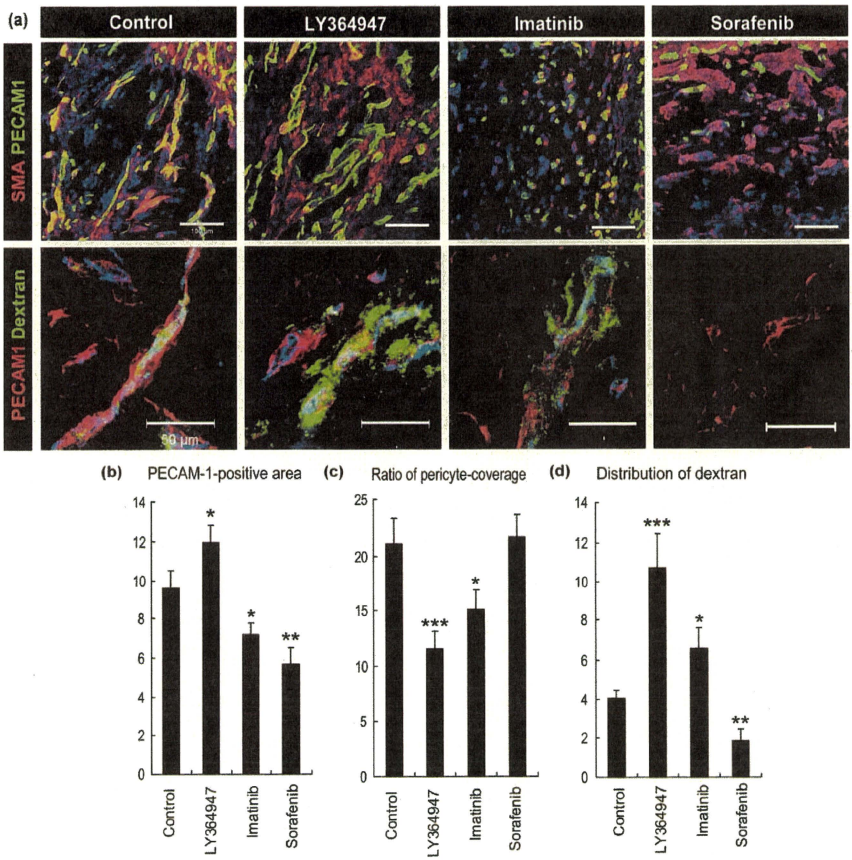


**Fig. 1.** The effects of three types of kinase inhibitors on extravasation of dextran in the Matrigel plug assay. (a) Confocal microscopy analyses. Upper row: staining of platelet endothelial cell adhesion molecule (PECAM)-1-positive endothelium in green and smooth muscle α-actin (SMA)-positive pericytes in red. Scale bars = 100 μm. Lower row: distribution of 2 MDa dextran in green and PECAM-1-positive endothelium in red. Scale bars = 50 μm. (b–d) Results of quantification ($n = 15$) of areas of endothelium (b, in percentage in one microscopic view), ratio of pericyte-covered endothelium (c, in percentage), and dextran distribution (d, in percentage in one microscopic view). Bars in the graphs represent standard errors. $^{*}P < 0.05$; $^{**}P < 0.01$; and $^{***}P < 0.001$.

heparin as angiogenic molecules to form mature neovasculature inside the gel plug, according to our previous report.[16] Of the two cancer models used in the present study, one was a well-established hypervascular cancer model using the murine colon cancer cell line CT26, whereas the other was an interstitium-rich cancer model using the human pancreatic cancer cell line BxPC3. With the latter model, we previously demonstrated therapeutic effects of combined use of TGF-β inhibitor on nanoparticles.[7] Using these models, we investigated the effects of SMWI on the distribution of 2 MDa dextran, a model of nanoparticles with an estimated hydrodynamic diameter of 50 nm.[6] The Matrigel plug assay and tumor model experiments revealed that TGF-β inhibitor increased extravasation of 2 MDa dextran in pericyte-covered neovasculature, whereas sorafenib increased that in vasculature with less pericyte coverage. These findings are important for determination of the optimal choice of angiogenic


doi: 10.1111/j.1349-7006.2008.01003.x

regulators in combination with nanoparticles for chemotherapy of cancer in general.

## Materials and Methods

**Reagents and antibodies.** TGF-β inhibitor was purchased from Calbiochem (San Diego, CA, USA; LY364947, catalog no. 616451), imatinib was from Novartis Pharma (Tokyo, Japan), and sorafenib was from Bayer Healthcare (West Haven, CT, USA). These compounds were diluted in dimethyl sulfoxide to 5, 25, and 10 mg/mL, respectively, as stock solutions. Fluorescein isothiocyanate (FITC)-conjugated dextran of 2 000 000 Da (2 MDa) was obtained from Sigma-Aldrich (St Louis, MO, USA). The antibody to platelet endothelial cell adhesion molecule (PECAM)-1 was from BD PharMingen (San Diego, CA, USA), that to NG2 was from Chemicon (Temecula, CA, USA), and that to smooth muscle α-actin (SMA) (Cy3-conjugated) was from Sigma-Aldrich. AlexaFluor-conjugated secondary antibodies were purchased from Invitrogen Molecular Probes (Eugene, OR, USA).

**Cancer cell lines and animals.** The BxPC3 human pancreatic adenocarcinoma cell line was obtained from the American Type Culture Collection (Manassas, VA, USA), and was grown in RPMI-1640 medium supplemented with 10% fetal bovine serum. The murine colon adenocarcinoma CT26 cell line was from the National Cancer Center Research Institute, Japan, and was cultured in Dulbecco's modified Eagle's medium (Sigma-Aldrich) containing 10% fetal bovine serum. BALB/c mice and BALB/c nude mice, 5–6 weeks of age, were obtained from Sankyo Laboratory (Tokyo, Japan) and Charles River Laboratories (Tokyo, Japan), respectively.

***In vivo* Matrigel plug assay and cancer models.** Matrigel plugs were created by mixing 0.2 mg/mL recombinant human VEGF-A (VEGF165; R & D Systems, Minneapolis, MN, USA), 1 mg/mL FGF-2 (R & D Systems), and 0.1 mg/mL heparin (Aventis Pharma, Tokyo, Japan) by pipetting, in combination with regular Matrigel (catalogue no. 354234; BD Biosciences, Franklin Lakes, NJ, USA). Matrigel (400 μL per plug; one plug per mouse) was injected subcutaneously into the abdominal region of BALB/c mice. Each Matrigel plug was harvested on day 7 and frozen directly in dry-iced acetone for immunohistochemistry. As cancer models, $5 \times 10^6$ BxPC3 cells or $1 \times 10^6$ CT26 cells were implanted by subcutaneous injection into the abdominal region of BALB/c nude and normal BALB/c mice and allowed to grow for 3 weeks and 1 week, respectively, until reaching the proliferative phase. For the *in vivo* permeability assay, TGF-β inhibitor at 1 mg/kg, imatinib at 50 mg/kg, or sorafenib at 40 mg/kg was administered as one shot intraperitoneally 18 h before injection of dextran. Dextran was administered intravenously via lateral tail veins 6 h before harvesting of samples. For perfusion study in the tumor tissues, dextran of 2 MDa was administered intravenously, at 24 h after SMWI-administration and 10 min before harvesting, and the excised samples were directly fixed in formalin. All experimental protocols were carried out in accordance with the policies of the Animal Ethics Committee at the University of Tokyo.

**Histology and immunohistochemistry.** The excised samples were either directly frozen in dry-iced acetone for immunohistochemistry, or fixed overnight in 4% paraformaldehyde and then paraffin embedded to prepare them for hematoxylin–eosin (HE) staining or perfusion study in the tumor tissues. Frozen samples were further sectioned at 10 μm thickness in a cryostat, briefly fixed with 10% formalin, and then incubated with primary and fluorescent secondary antibodies. Samples were observed with a LSM510 Meta confocal microscope (Zeiss, Thornwood, NY, USA) for immunohistochemistry, and with an AX80 microscope (Olympus, Tokyo, Japan) for HE staining.

**Quantification.** Areas in Matrigel plugs that were PECAM-1-positive, double-positive for PECAM-1 and SMA, and FITC–dextran-positive in confocal micrographs ($n = 15$), or lengths of FITC–dextran-positive structure in the tumor tissues ($n = 12$) were measured using Adobe Photoshop software (Adobe Systems, San Jose, CA, USA) and ImageJ software (freeware distributed by the National Institutes of Health, USA). Pericyte coverage was quantified as the ratio of PECAM-1/SMA-double-positive areas to PECAM-1-positive areas, as described previously.[7] Results were further analyzed statistically by Student's *t*-test using Microsoft Excel software (Microsoft, Redmond WA, USA).

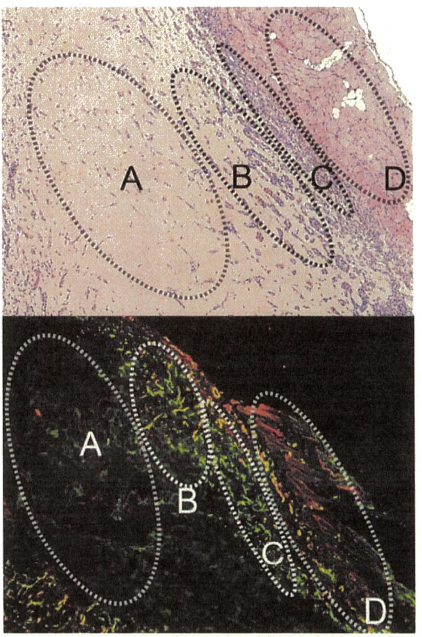


**Fig. 2.** Low-magnification view of the Matrigel plug and surrounding regions in sections with hematoxyline-eosin (HE) staining (upper) and with immunohistochemistry (lower). (a) Avascular area, (b) vascularized intraplug region, (c) periplug region, and (d) normal tissue. Green, platelet endothelial cell adhesion molecule-1; red, smooth muscle α-actin.

## Results

We initially carried out the Matrigel plug assay *in vivo*, in which regular Matrigel was mixed with VEGF-A, FGF-2, and heparin[16] to investigate the effects of three SMWI on the extravasation of 2 MDa dextran (Fig. 1). Marked induction of pericyte-covered mature neovasculature was observed in the gel plug after a 7-day incubation in mice, as we reported previously.[16] Pericytes were determined to be SMA-positive cells in a Matrigel plug assay. In this model, administration of TGF-β inhibitor decreased pericyte coverage of the neovasculature and significantly enhanced the distribution of 2 MDa dextran. This observation was consistent

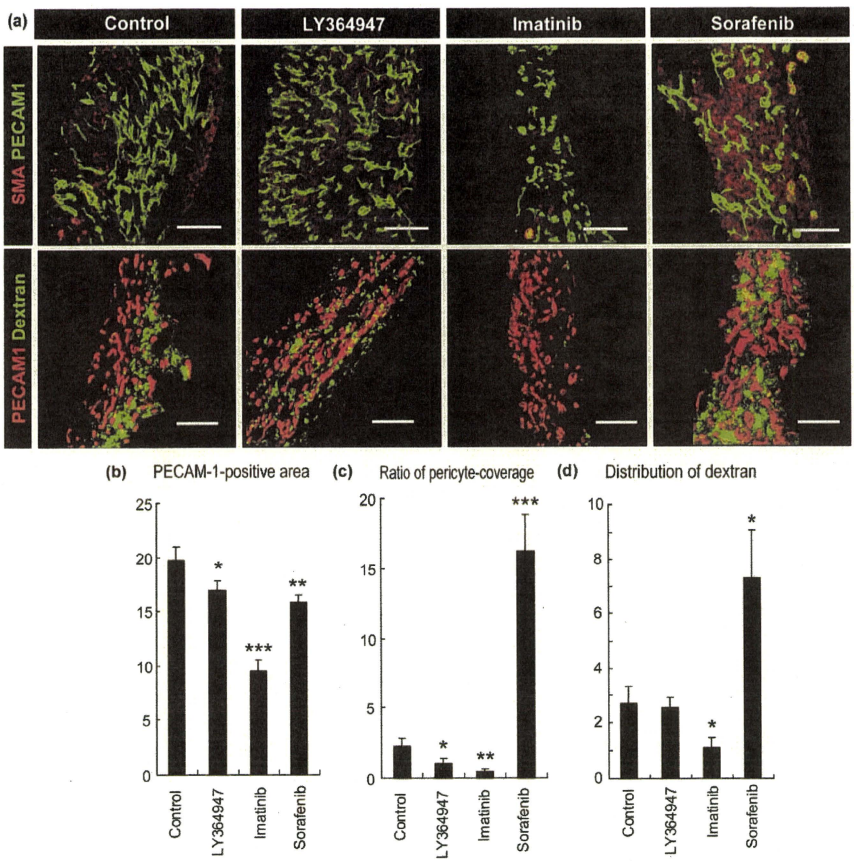


**Fig. 3.** Effects of three types of kinase inhibitors on extravasation of dextran from vasculature in the periplug region. (a) Confocal microscopy analyses. Upper row: staining of platelet endothelial cell adhesion molecule (PECAM)-1-positive endothelium in green and smooth muscle α-actin (SMA)-positive pericytes in red. Lower row: distribution of 2 MDa dextran in green and PECAM-1-positive endothelium in red. Scale bars = 100 μm. (b–d) Results of quantification ($n$ = 15) of areas of endothelium (b, in percentage in one microscopic view), ratio of pericyte-covered endothelium (c, in percentage), and dextran distribution (d, in percentage in one microscopic view). Bars in the graphs represent standard errors. $^{*}P < 0.05$; $^{**}P < 0.01$; and $^{***}P < 0.001$.

with our previous study, in which we used animal models of pancreatic adenocarcinoma and diffuse-type gastric cancer.[7] Based on this result, we expected that a decrease in pericytes might induce more extravasation of 2 MDa dextran.

To confirm this, we compared the effects of imatinib administration, which inhibits PDGF signaling and may therefore decrease pericyte coverage. However, administration of imatinib decreased the total accumulation of 2 MDa dextran compared with TGF-β inhibitor (Fig. 1). Although imatinib actually decreased pericyte coverage to the same level of TGF-β inhibitor, it also decreased PECAM-1-positive endothelium together with pericyte coverage. These findings of morphological analysis were consistent with those noted in a previous report.[17] TGF-β inhibitor maintained the area of PECAM-1-positive endothelium and may therefore be superior to imatinib. In addition, although VEGF inhibition was expected to increase drug delivery, based on the


doi: 10.1111/j.1349-7006.2008.01003.x

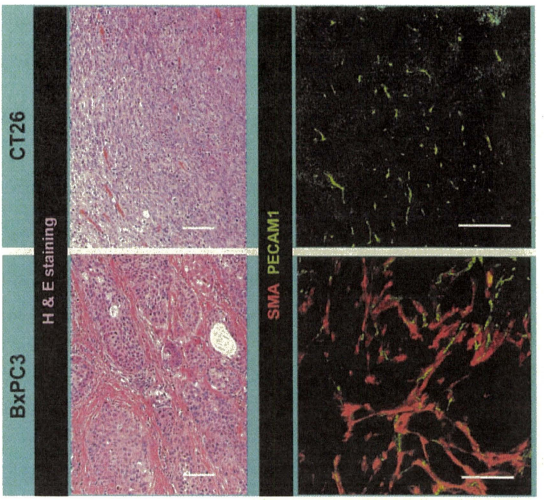


**Fig. 4.** Two animal tumor models using CT26 and BxPC3 cell lines. Histological examination of tumor models by hematoxylin–eosin staining and immunohistochemistry with platelet endothelial cell adhesion molecule (PECAM)-1 in green and smooth muscle α-actin (SMA) in red. Scale bars = 100 μm.

results of previous studies,[8] sorafenib nearly eliminated the influx of 2 MDa dextran and resulted in far less accumulation of it. This result can be explained by the potent reduction of PECAM-1-positive endothelium and increase in pericytes as sleeves. These morphological changes induced by VEGF inhibition were also consistent with previous reports.[18]

Although the neovasculature inside the gel plugs was as described above, the vasculature in the regions surrounding the gel plugs, or sites of acute inflammation in reaction to the plugs as foreign bodies (Fig. 2), exhibited different patterns. Compared to the vasculature inside the gel plug, that in regions around the plugs was denser and more tortuous, and was accompanied by pericytes to a smaller extent. These phenotypes resembled those of the vasculature in conventional animal models of tumors, such as the CT26 model, as we describe later in this report. We termed these two regions the 'intraplug' and 'periplug' regions, respectively, after the established terminology in oncology, 'intratumoral' and 'peritumoral'.

Functionally, the vasculature in periplug regions was leaky to 2 MDa dextran in the control condition, that is, without any modulation by SMWI (Fig. 3). Surprisingly, the effects of SMWI on neovasculature in the periplug regions were quite different from those in the intraplug regions. In the periplug regions, pericyte coverage of the neovasculature was far less than in the intraplug region, even in the control condition. In this periplug region, neither TGF-β inhibitor nor imatinib significantly altered pericyte coverage. Consequently, these compounds did not alter the accumulation of 2 MDa dextran. Sorafenib, on the other hand, did increase pericyte coverage, and increased the accumulation of 2 MDa dextran. This increase in extravasation was consistent with previous reports on the effects of VEGF inhibition.[8]

We subsequently compared these findings in the Matrigel plug assay with those in two subcutaneous tumor xenograft models. We used the CT26 cell line derived from murine colon cancer and the BxPC3 cell line derived from human pancreatic adenocarcinoma (Fig. 4). HE staining of CT26 xenografts revealed a well-vascularized medullary histological pattern with little tumor stroma, whereas that of BxPC3 xenografts revealed a stroma-rich histology. Immunostaining of PECAM-1 and SMA confirmed this stroma-rich characteristic of the BxPC3 model. Although the BxPC3 model grew more slowly than the CT26 model, the BxPC3 model also reached the proliferative phase. Compared to the BxPC3 model, the CT26 model required one-fifth of the number of inoculating cells and one-third of the duration to reach the proliferative phase, which was 1 week for the CT26 model and 3 weeks for the BxPC3 model (data not shown). These differences may well be due to the differences in requirements for induction of stromal components from host animals, as well as rates of proliferation of tumor cell lines.

We then tested the alterations in vascular phenotypes as well as accumulation of 2 MDa dextran with or without SMWI in these tumor models (Fig. 5). We here used NG2 as the pericyte marker (Fig. 5a), because SMA-positive cells (i.e. myofibroblasts) are abundant especially in the stroma of BxPC3 tumor (Fig. 4). In the CT26 model, sorafenib did increase the pericyte-covered vasculature, whereas other SMWI did not increase the pericytes. Imatinib decreased endothelial cells. These observations in the CT26 tumor model were consistent with those in the periplug region of the Matrigel plug. In the BxPC3 model, pericyte coverage was less with LY364947 and imatinib, and endothelial cells were decreased with imatinib and sorafenib. These findings in the BxPC3 tumor model were consistent with those in the intraplug region. Accordingly, 2 MDa dextran was diffusely distributed in tumor tissue without any treatment in the CT26 model, whereas almost no leakage of dextran was observed in the BxPC3 model (Fig. 5b). Sorafenib exhibited the best effect in the CT26 model, whereas TGF-β inhibitor did in the BxPC3 model. The latter result was consistent with the findings of our previous work using nanoparticles including PEGylated liposomes incorporating doxorubicin (Doxil) of approximately 100 nm in diameter, which exhibited antitumor effects in the BxPC3 model

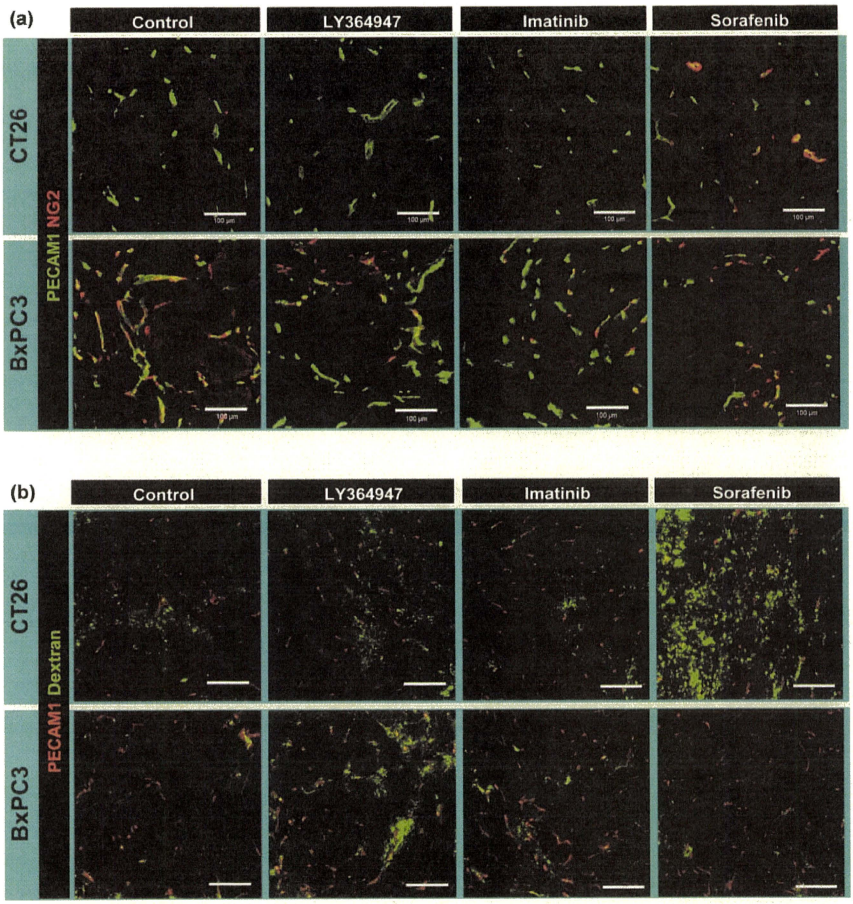


**Fig. 5.** Effects of three kinase inhibitors in the tumor models. (a) Vascular phenotypes revealed by immunohistochemistry. Green, platelet endothelial cell adhesion molecule (PECAM)-1; red, NG2. (b) Extravasation of 2 MDa dextran from vasculature. Dextran in green and PECAM-1 in red. Scale bars = 100 μm.

only when combined with TGF-β inhibitor.[7] We also tested the effects of Doxil with or without TGF-β inhibitor in the CT26 model. Monotherapy with Doxil at 8 mg/kg almost completely inhibited tumor growth, and combined administration of TGF-β inhibitor did not yield any significant additional effects (data not shown). These findings were consistent with those observed in the Matrigel plug assay. The effects of combined use of imatinib were also consistent with those in the Matrigel plug assay.

Increased accumulation of dextran in these tumor models at 7 h after injection, by sorafenib in the CT26 tumor and by LY364947 in the BxPC3 tumor, can also be explained by an increase in the amount of vasculature with perfusion, not only by an increase in leakage. To test this possibility, we examined changes in perfusion by intravascular existence of dextran at only 10 min after administration, because dextran of 2 MDa should basically remain inside vasculature at that time after



doi: 10.1111/j.1349-7006.2008.01003.x

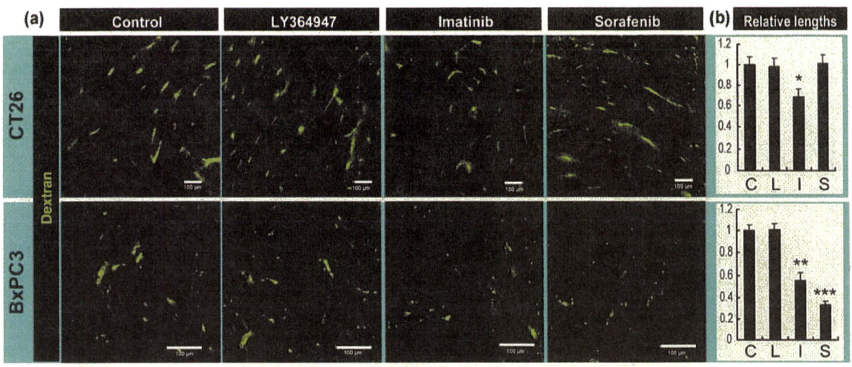


**Fig. 6.** Perfusion study in the tumor models. (a) Tumor vessels with perfusion were determined by the existence of dextran in green, administrated at 10 min before harvesting. Scale bars = 100 μm. (b) Relative lengths of vessels with perfusion. C, control; I, imatinib; L, LY364947; S, sorafenib. Bars represent standard errors. $*P < 0.05$; $**P < 0.01$; and $***P < 0.001$.

injection.[6] As shown in Figure 6, the lengths of vasculature with blood flow were not altered in the conditions exhibiting increased accumulation of dextran, that is, by sorafenib treatment in the CT26 tumor and by LY364947 treatment in the BxPC3 tumor. Therefore, the increased accumulation of dextran in these conditions may largely be due to an increase in vascular leakiness.

## Discussion

We have previously shown that use of short-acting SMW TGF-β inhibitor can increase the distribution of nanoparticles in stroma-rich tumors by increasing the leakiness of the tumor neovasculature.[7] By virtue of the brief duration of SMWI effects, potential side effects can be decreased due to long-term suppression of essential signaling pathways. There are still a number of SMWI that can be used for manipulation of tumor neovasculature via their effects on pericytes or endothelium. We therefore compared the effects of two of these SMWI, imatinib and sorafenib.

Combined use of VEGF inhibition has been reported to have potent effects on drug delivery into tumor tissues.[19] The underlying mechanism for this has been explained by the vascular 'normalization' theory,[8] or decreased interstitial fluid pressure by decreased leakiness of tumor vasculature, via a decrease in endothelial cells and increase in pericyte coverage. Consistent with this, VEGF inhibition by sorafenib had significant effects on the retention of 2 MDa dextran in the periplug regions and in CT26 tumor, where vasculature showed less pericyte coverage and denser endothelium than in normal tissues. However, VEGF inhibition significantly decreased retention of the same dextran in adjacent areas, the intraplug region, and in BxPC3 tumor. Vascular phenotypes in these regions were characterized by more pericyte coverage and sparser endothelium, that is, they were more 'normal' than those in the periplug region and in CT26 tumor.

One of the differences between these two kinds of vasculature was the blood flow in the vasculature after sorafenib treatment. In CT26 tumor after sorafenib treatment, blood flow was maintained, whereas the flow ceased in sorafenib-treated BxPC3 tumor. These differences may partially be because of differences in sensitivity of the endothelium to the change in VEGF signaling, known to be at least due to differences in expression levels of VEGFR2.[18]

Another apparent difference in these tumor models was pericyte coverage before drug administration. Less pericyte coverage has been reported to result in more leakiness.[11–13] The degrees of dextran accumulation in all control conditions (i.e. without modification by SMWI) are consistent with the degrees of pericyte coverage. Increased dextran accumulation in LY364947-treated BxPC3 tumors can also be explained by decreased pericyte coverage, not by normalization. Both blood perfusion (Fig. 6) and interstitial fluid pressure, which we previously reported,[7] did not differ with or without LY364947 treatment in BxPC3 tumor. These findings suggest that we may need different approaches, such as the use of TGF-β inhibitor to increase drug delivery (at least for nanoparticles), to develop effective treatment for tumors with originally 'more normal' tumor vasculature. Note, however, that these more normal vessels in tumors might not be completely normal, because TGF-β inhibitor did not alter the accumulation of nanoparticles in true normal tissues, as we previously reported.[7]

Regarding the degree of original pericyte coverage in tumor vasculature, an increase in the amount of stromal components in tumor tissue may result in an increase in pericyte coverage. In a previous study, we found that the presence of FGF-2 together with VEGF-A enhances mature neovascularization compared with VEGF-A alone.[16] In addition to FGF-2, a set of signaling molecules is needed to recruit and to induce proliferation of pericytes. These include PDGF-BB[12,13] (homodimer of PDGF-B chain) and TGF-β.[11,20] These signaling molecules are reported to be secreted from components of the tumor stroma and, above all, cancer-associated fibro-blasts[21–23] and macrophages.[24] Tumors with more stroma, including fibroblasts and immune cells, have more pericyte coverage of the vasculature with greater maturity and less leakiness. Although chemoresistance of tumors has been largely investigated from the aspect of drug sensitivity of tumor cells per se, it is possible that the histological pattern of the tumor tissues may also constitute a reason for chemoresistance, because of insufficient drug delivery to the tumor cells.

The Tie2–angiopoietin signaling pathway is also known to be involved in vessel maturation and to affect pericytes.[25] Because there are no SMW compounds available to inhibit this signaling pathway, we tested the effects of one-shot Tie2-Fc chimeric

protein at 50 mg/kg bodyweight with 2 MDa dextran in the Matrigel plug assay, but no significant effects on accumulation of 2 MDa dextran were observed (M.R. Kano, unpublished data, 2008). There are two possible explanations for this observation: spatial and temporal. According to the spatial explanation, because Tie2–angiopoietin signaling occurs between the endothelium and pericytes and thus outside the vessel lumen, the Fc chimera, which is of fairly large molecular size and may therefore be retained inside vessel lumens, is not able to affect signaling. The other drugs used in the present study were all SMWI, which may easily exit the vessel lumen and penetrate the perivascular tissues. The second explanation is temporal. Although this signaling pathway is known to be deeply involved in development, whether it is also involved in the maintenance of endothelial-mural structure is not known. Because we observed the effects of drugs only at 24 h after administration, it is possible that other inhibitors inhibited only the maintenance functions of the signaling pathways, and not functions related to development. Administration of TGF-β inhibitor did not significantly affect the vasculature in normal organs,[7] so it is possible that the neovasculature requires larger amounts of signaling molecules to maintain structure than do established vessels.

In conclusion, the appropriate strategy for optimization of tumor vasculature for drug delivery system using nanoparticles may not be uniform, and may depend on tumor type, including differences in the degree of pericyte coverage of tumor vasculature.

## Acknowledgments

We thank Dr Peter Baluk, Cardiovascular Research Institute, University of California, San Francisco (UCSF), for advice about perfusion. This work was supported by Grant-in-Aid for Scientific Research (KAKENHI 19790282 and 17016011) from the Ministry of Education, Culture, Sports, and Technology of Japan (MEXT), and a Health Labor Sciences Research Grant from the Ministry of Health, Labor, and Welfare of Japan.

## References

1 Giroux V, Malicet C, Barthet M *et al.* p8 is a new target of gemcitabine in pancreatic cancer cells. *Clin Cancer Res* 2006; **12**: 235–41.
2 Merriman RL, Hertel LW, Schultz RM *et al.* Comparison of the antitumor activity of gemcitabine and ara-C in a panel of human breast, colon, lung and pancreatic xenograft models. *Invest New Drugs* 1996; **14**: 243–7.
3 Rothenberg ML, Moore MJ, Cripps MC *et al.* A phase II trial of gemcitabine in patients with 5-FU-refractory pancreas cancer. *Ann Oncol* 1996; **7**: 347–53.
4 Hanahan D, Weinberg RA. The hallmarks of cancer. *Cell* 2000; **100**: 57–70.
5 Jain RK. Physiological barriers to delivery of monoclonal antibodies and other macromolecules in tumors. *Cancer Res* 1990; **50**: 814S–19S.
6 Dreher MR, Liu W, Michelich CR, Dewhirst MW, Yuan F, Chilkoti A. Tumor vascular permeability, accumulation, and penetration of macromolecular drug carriers. *J Natl Cancer Inst* 2006; **98**: 335–44.
7 Kano MR, Bae Y, Iwata C *et al.* Improvement of cancer-targeting therapy, using nanocarriers for intractable solid tumors by inhibition of TGF-β signaling. *Proc Natl Acad Sci USA* 2007; **104**: 3460–5.
8 Jain RK. Normalization of tumor vasculature: an emerging concept in antiangiogenic therapy. *Science* 2005; **307**: 58–62.
9 Wilhelm S, Carter C, Lynch M *et al.* Discovery and development of sorafenib: a multikinase inhibitor for treating cancer. *Nat Rev Drug Discov* 2006; **5**: 835–44.
10 Bergers G, Song S. The role of pericytes in blood-vessel formation and maintenance. *Neuro Oncol* 2005; **7**: 452–64.
11 von Tell D, Armulik A, Betsholtz C. Pericytes and vascular stability. *Exp Cell Res* 2006; **312**: 623–9.
12 Abramsson A, Lindblom P, Betsholtz C. Endothelial and nonendothelial sources of PDGF-B regulate pericyte recruitment and influence vascular pattern formation in tumors. *J Clin Invest* 2003; **112**: 1142–51.
13 Lindblom P, Gerhardt H, Liebner S *et al.* Endothelial PDGF-B retention is required for proper investment of pericytes in the microvessel wall. *Genes Dev* 2003; **17**: 1835–40.
14 Buchdunger E, Zimmermann J, Mett H *et al.* Inhibition of the Abl protein-tyrosine kinase *in vitro* and *in vivo* by a 2-phenylaminopyrimidine derivative. *Cancer Res* 1996; **56**: 100–4.
15 Bergers G, Song S, Meyer-Morse N, Bergsland E, Hanahan D. Benefits of targeting both pericytes and endothelial cells in the tumor vasculature with kinase inhibitors. *J Clin Invest* 2003; **111**: 1287–95.
16 Kano MR, Morishita Y, Iwata C *et al.* VEGF-A and FGF-2 synergistically promote neoangiogenesis through enhancement of endogenous PDGF-B–PDGFRβ signaling. *J Cell Sci* 2005; **118**: 3759–68.
17 Vlahovic G, Rabbani ZN, Herndon JE, Dewhirst MW, Vujaskovic Z. Treatment with Imatinib in NSCLC is associated with decrease of phosphorylated PDGFR-β and VEGF expression, decrease in interstitial fluid pressure and improvement of oxygenation. *Br J Cancer* 2006; **95**: 1013–19.
18 Mancuso MR, Davis R, Norberg SM *et al.* Rapid vascular regrowth in tumors after reversal of VEGF inhibition. *J Clin Invest* 2006; **116**: 2610–21.
19 Hurwitz H, Fehrenbacher L, Novotny W *et al.* Bevacizumab plus irinotecan, fluorouracil, and leucovorin for metastatic colorectal cancer. *N Engl J Med* 2004; **350**: 2335–42.
20 Hirschi KK, Rohovsky SA, D'Amore PA. PDGF, TGF-β, and heterotypic cell–cell interactions mediate endothelial cell-induced recruitment of 10T1/2 cells and their differentiation to a smooth muscle fate. *J Cell Biol* 1998; **141**: 805–14.
21 Pietras K, Pahler J, Bergers G, Hanahan D. Functions of paracrine PDGF signaling in the proangiogenic tumor stroma revealed by pharmacological targeting. *PLoS Med* 2008; **5**: e19.
22 Micke P, Ostman A. Tumour–stroma interaction: cancer-associated fibroblasts as novel targets in anti-cancer therapy? *Lung Cancer* 2004; **45**: S163–75.
23 Bhowmick NA, Moses HL. Tumor–stroma interactions. *Curr Opin Genet Dev* 2005; **15**: 97–101.
24 Lewis CE, Pollard JW. Distinct role of macrophages in different tumor microenvironments. *Cancer Res* 2006; **66**: 605–12.
25 Armulik A, Abramsson A, Betsholtz C. Endothelial/pericyte interactions. *Circ Res* 2005; **97**: 512–23.



doi: 10.1111/j.1349-7006.2008.01003.x